



Published in final edited form as:

J Med Chem. 2022 November 24; 65(22): 15457–15472. doi:10.1021/acs.jmedchem.2c01418.

Development of fluorinated peptoid-based histone deacetylase (HDAC) inhibitors for therapy-resistant acute leukemia

Nina Reißing^{‡,1,2}, Julian Schliehe-Diecks^{‡,3}, Paris R. Watson⁴, Melf Sönnichsen³, Abigail D. Cragin⁴, Andrea Schöler², Jing Yang^{3,5}, Linda Schäker-Hübner¹, Arndt Borkhardt³, David W. Christianson⁴, Sanil Bhatia³, Finn K. Hansen¹

¹Pharmaceutical Institute, Pharmaceutical and Cell Biological Chemistry, University of Bonn, Ander Immenburg 4, 53121 Bonn, Germany

²Institute for Drug Discovery, Medical Faculty, Leipzig University, Brüderstraße 34, 04103 Leipzig, Germany

³Department of Pediatric Oncology, Hematology and Clinical Immunology, Medical Faculty, Heinrich Heine University Düsseldorf, Moorenstr. 5, 40225 Düsseldorf, Germany

⁴Roy and Diana Vagelos Laboratories, Department of Chemistry, University of Pennsylvania, 231 South 34th Street, Philadelphia, Pennsylvania 19104-6323, United States

⁵Department of Medicine, Yangzhou Polytechnic College, West Wenchang Road 458, Yangzhou, 225009, P.R. China

Abstract

Using a microwave-assisted protocol, we synthesized sixteen peptoid-capped HDAC inhibitors (HDACi) with fluorinated linkers and identified two hit compounds. In biochemical and cellular assays, **10h** stood out as a potent unselective HDACi with remarkable cytotoxic potential against different therapy resistant leukemia cell lines. Of note, **10h** demonstrated prominent antileukemic activity with low cytotoxic activity toward healthy cells. Moreover, **10h** exhibited synergistic interactions with the DNA methyltransferase inhibitor decitabine in AML cell lines. The comparison of crystal structures of HDAC6 complexes with **10h** and its non-fluorinated counterpart revealed a similar occupation of the L1 loop pocket but slight differences in the zinc coordination. The substitution pattern of the acyl residue turned out to be crucial in terms

Corresponding Author: F.K.H.: phone, (+49) 228 73 5213; fax, (+49) 228 73 7929; finn.hansen@uni-bonn.de.; S.B.: phone, (+49) 211 81 04896; fax, (+49) 211 81 16436; sanil.bhatia@med.uni-duesseldorf.de.

[‡]Author Contributions

N.R. and J.S.-D. share the first authorship. S.B. and F.K.H. contributed equally to this work as senior authors. N.R. synthesized all intermediates and target compounds. P.R.W., A.D.C., and D.W.C. determined the crystal structure of the HDAC6-**10h** complex. J.S.-D., M.S., A.S., J.Y., and L.S.-H. performed the biological evaluation. A.B., D.W.C., S.B., and F.K.H. acquired funding and provided resources. N.R., S.B. and F.K.H. designed the study. The manuscript was written through contributions of all authors. All authors have given approval to the final version.

Supporting Information

The Supporting Information is available free of charge on the ACS Publications website. Supplementary tables, NMR spectra, and HPLC traces of newly synthesized compounds. (PDF) Molecular formula strings and some data. (CSV)

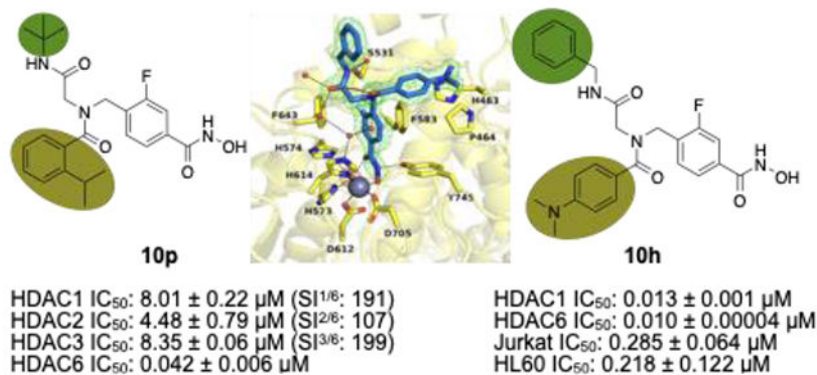
Accession Code

The atomic coordinates and crystallographic structure factors of the HDAC6-**10h** complex have been deposited in the Protein Data Bank (www.rcsb.org) with accession code 7U8Z. Authors will release the atomic coordinates upon article publication.

The authors declare no competing financial interest.

of isoform selectivity. The introduction of an isopropyl group to the phenyl ring provided the highly HDAC6 selective inhibitor **10p** which demonstrated moderate synergy with decitabine and outmatched the HDAC6 selectivity of tubastatin A.

Graphical Abstract



Keywords

Histone deacetylase; cancer; leukemia; synergism; fluorination

INTRODUCTION

Epigenetic events are largely induced by environmental factors and determine the post-translational alteration of a cell phenotype.¹ In today's drug discovery, controlling epigenetic mechanisms by regulating histone modifications such as histone acetylation, methylation or phosphorylation is of growing importance.^{1,2} One group of enzymes involved in such processes are histone deacetylases (HDACs) which have attracted attention as promising targets for cancer therapy. Consisting of eleven zinc-dependent isoforms and the NAD⁺-dependent sirtuins, the HDAC family is divided into classes I–IV.³ Among those, only the class I isoforms HDAC1–3 control the acetylation levels of histones, thus modifying the chromatin structure and its accessibility for gene transcription.³ Other isoforms participate in a variety of biological processes such as the formation of protein-protein complexes, the mediation of immunosuppression via Forkhead box P3 (Foxp3) deacetylation, and the regulation of transcription factors.^{4,5,6,7} HDAC inhibitors (HDACi) typically comprise a capping group occupying the outside of the enzyme's active site, a zinc-binding group chelating the catalytically active zinc ion, and a linker chain connecting the two parts. Resulting from the highly conserved nature of the enzymes, this pharmacophore model generally applies to all isoforms, including the class I enzymes.³ Being particularly cytotoxic due to their interference with cell cycle progression and proliferation, selective class I HDACi as well as pan-inhibitors are considered promising tools for the therapy of both hematological and solid tumors.⁸ Since their discovery, four HDACi, e.g. vorinostat, belinostat, panobinostat, and the class I-selective natural compound romidepsin, have been FDA-approved to treat hematological cancers, including multiple myeloma and T cell lymphoma.^{6,8,9} The class I-selective tucidinostat has recently become the first HDACi to

be approved for the therapy of solid tumors by the NMPA in China.¹⁰ Another field of interest concerning class I HDACi on clinical level is their presumed ability to eradicate latent HIV reservoirs.¹¹

Despite their potential in cancer therapy, pan-HDACi are typically associated with adverse effects. To explore the scope beyond oncology, the research on isoform-specific HDACi with reduced off-target interactions and higher tolerability is quickly evolving.⁸ The most promising target for isoform-selective inhibition with improved safety profiles is HDAC6, which appears to play a role in cancer, neurodegenerative diseases, inflammation, rheumatoid arthritis, and neurological disorders.^{12,13,14,15,16,17} The first HDAC6-preferential drug candidate ricolinostat (phase II), its chlorinated analog citarinostat (phase I), and several yet undisclosed HDAC6i considered for non-oncological conditions (phase II) are currently being assessed in clinical trials.¹⁸ Unlike other isoforms, the class IIb isoform HDAC6 is located in the cytoplasm instead of the nucleus and comprises two catalytic domains (CDs).^{19,20} One of which, CD1, is considered inactive toward histones while its biological role remains unclear.²¹ Confirmed substrates of the second catalytic domain (CD2) include α -tubulin and cortactin, which are both required for cytoskeleton formation; tau, and the chaperone protein Hsp90.^{21,22,23,24,25,26} HDAC6 is furthermore unique in comprising a ubiquitin-binding domain which regulates the aggresome-autophagy pathway as an important protein degradation system beside the 26S proteasome.^{27,28} Although recent studies imply only moderate cytotoxicity induced by selective HDAC6 inhibition²⁹, the enzyme remains a relevant drug target with high eligibility for combination therapies.³⁰

Supposedly triggering a beneficial alteration in gene expression patterns, the combination of HDACi and DNA-hypomethylating agents is another field of interest.³¹ The concurrent application of HDACi and decitabine in diffuse large B-cell lymphoma cell lines appeared to induce time-dependent synergistic effects resulting in tumor growth inhibition and increased apoptosis levels that exceeded the effect of HDACi alone.³¹ Other preclinical experiments hinted at synergistic effects activated by vorinostat and decitabine in mantle cell lymphoma and pancreatic cancer cell lines.^{31,32,33} Succeeding prior clinical trials on a pan-HDACi as an additive to decitabine, current studies are focusing on the class I-selective HDACi tucidinostat in lymphoma patients.^{34,35,36}

A feature with increasing prevalence in modern pharmaceuticals is fluorine. Although rarely occurring in natural compounds, fluorination has become an important means to improve the bioavailability and pharmacokinetic properties of drugs.³⁷ After adding up to 20–25% of all pharmaceuticals a decade ago, fluorinated drugs now account for one half of all blockbuster drugs.^{37,38} Compared to non-fluorinated analogs, the low polarization of the C-F bond and the high electron-withdrawing capabilities of fluorine substituents may significantly alter the pK_a, the lipophilicity, and the metabolic stability of drugs.^{37,39,40} Conformational changes due to the characteristic steric demands of fluorinated groups could have an additional impact on the binding mode and the target affinity.^{37,39,40} Indeed, another notable benefit of drug fluorination is the possibility of ¹⁸F radiolabelling. Apart from diagnostic measures, PET-tracing of ¹⁸F-labelled compounds can be useful for biodistribution studies of early-stage drug candidates, thus facilitating the drug development process.³⁷ Despite such advantages, fluorinated drugs bear the risk of high intrinsic toxicity owing to the

release of fluorine-containing metabolites.^{41,42} A careful investigation of the metabolic behavior of each fluorinated drug candidate is therefore inevitable.⁴¹

In 2016, our group published results on selective HDAC6 inhibition by peptoid-based compounds obtained by the Ugi 4-component reaction (U4CR).⁴³ Follow-up studies using co-crystals of selected peptoid-capped inhibitors in complex with the CD2 of *Danio rerio* (zebrafish) HDAC6 (α CD2) revealed that the compounds adopt different binding modes than the highly HDAC6-selective PET-probe bavarostat which carries a fluorine substituent in *m*-position to the hydroxamate in the otherwise identical linker moiety.^{44,45} Given that bavarostat and the unselective HDACi [¹¹C]martinostat, a cinnamoyl-based PET probe in clinical phase I, share identical cap groups, we concluded that the remarkable HDAC6-selectivity of bavarostat is likely to derive from the unique binding mode of the fluorinated linker moiety.⁴⁶ Moreover, a recent study of inhibitors similarly fluorinated and difluorinated at the *meta* positions of phenyl linker groups found that the compounds also exhibit HDAC6 selectivity, possibly due to interactions between the fluorine atoms and His361, Gly582, and Ser531 in loop pockets L1 and L2.⁴⁷ Based on the observation that selectivity profiles can be steered through substitution patterns in the cap group area, we decided to investigate the effect of linker fluorination on scaffolds that had previously turned out to favor either HDAC6- or pan-inhibition. The resulting set of highly potent, fluorinated HDACi were then assessed in respect of their antileukemic properties.

RESULTS AND DISCUSSION

Design and Synthesis.

Aiming to determine whether the bavarostat-inspired linker fluorination would improve the inhibitory qualities of our previously reported peptoids, we designed a new set of compounds that includes fluorinated analogs of the non-selective compounds DDK115 and DDK137 as well as the HDAC6-preferential inhibitors **Ie** and **IIf** (Scheme 1).^{45,48} In a recent study on tetrazole-capped HDACi derived from the peptoid-scaffold, we moreover identified the 2-trifluoromethyl substituent of the acyl moiety as a source of excellent selectivity.⁴⁹ An additional SAR study therefore featured several analogs with differently shaped substituents in the same position.

The synthesis of the 2-fluorophenyl linker was performed in accordance with a literature protocol (Scheme 2).⁵⁰ Following the esterification of **1**, NBS was used to introduce a bromine substituent (**3**) which was then substituted to give the corresponding azide **4**. Next, the Staudinger reaction using triphenylphosphine was carried out to afford the desired amine, which was easily isolated as the hydrochloride salt **5**. The U4CR of **5**, the respective isonitriles **6**, the respective carboxylic acids **7**, and paraformaldehyde **8** built the peptoid scaffolds **9** within less than 4 hours of microwave irradiation (Scheme 3). After aqueous workup and recrystallization of the crude products, the resulting esters **9** were treated with a mixture of sodium hydroxide and aqueous hydroxylamine to yield the hydroxamates **10** after 15 min of stirring at 0 °C. All final compounds were isolated by precipitation from the aqueous crude mixture and exceeded 95% purity without further purification.

HDAC inhibition.

Biochemical assays were performed to evaluate the inhibitory activities of all final compounds against HDAC1 and HDAC6. The resulting IC₅₀ values (Table 1) indicate that minor structural modifications suffice to steer between unselective inhibition and HDAC6 selectivity without affecting the overall high inhibitory activities against HDAC6 in the low nanomolar concentration range. In comparison to compounds featuring a cyclohexyl group in position R¹ (**10c-f**; IC₅₀ HDAC6: 0.018–0.020 μM, selectivity indices (SI^{HDAC1/6}): 43–75), it is apparent that the *tert*-butyl derivatives **10k-n** with identical substitution patterns at the R² moiety display more promising selectivity profiles (SI^{HDAC1/6}: 45–103) and similar potencies (IC₅₀ HDAC6: 0.017–0.027 μM). The selectivity profile of the voluminous and branched *iso*-propyl derivative **10p** (SI^{HDAC1/6}: 191) exceeded all other analogs as well as the control compound tubastatin A (SI^{HDAC1/6}: 178), in spite of the slightly impaired inhibition of HDAC6 (0.042 μM). Hence, **10p** was singled out as the most selective inhibitor of this set. The equally bulky 2-chloro analog **10o** was found to be twice as potent (IC₅₀ HDAC6: 0.021 μM) but less selective (SI^{HDAC1/6}: 165). Additional assays using HDAC2 and HDAC3 confirmed the low activity of **10p** against other class I isoforms (IC₅₀ HDAC2: 4.48 μM, SI^{HDAC2/6}: 107; HDAC3: 8.35 μM, SI^{HDAC3/6}: 199). Furthermore, we screened **10p** against HDAC4 as a representative class IIa isoform. As expected, the compound turned out to be inactive (IC₅₀ HDAC4: > 10 μM, SI^{HDAC4/6}: > 238; Figure 1).

In accordance with previous SAR data, all inhibitors featuring 3,5-dimethyl residues in the acyl ring (**10a**, **10g**, **10i**) exhibited only low to moderate HDAC6 selectivity (SI^{HDAC1/6}: 6–24) but high inhibitory qualities ranging from 0.013 μM to 0.024 μM against HDAC6.^{48,51} The two 4-dimethylamino derivatives **10b** and **10h** met the expectations by turning out to be strong unselective inhibitors (SI: 1.4–8) of which **10h** proved to be the most potent ligand against both isoforms (IC₅₀ HDAC1: 0.013 μM; HDAC6: 0.010 μM) and other class I enzymes (IC₅₀ HDAC2: 0.014 μM, SI^{HDAC2/6}: 1.4; HDAC3: 0.021 μM, SI^{HDAC3/6}: 2.1; Figure 1). Compound **10h** also displayed some inhibitory activity against HDAC4 (IC₅₀ HDAC4 1.88 μM, SI^{HDAC4/6}: 188; Figure 1). The *tert*-butyl-capped analog **10j** (IC₅₀ HDAC1: 0.158 μM; HDAC6: 0.020 μM, SI: 7.9) exhibited similar inhibition qualities as ricolinostat. In summary, those results indicate that the substitution pattern of the acyl ring is crucial in terms of isoform selectivity. Depending on the size of the residue, the sole occupation of position 2 of the aromatic ring promises a strong preference for HDAC6. The introduction of small residues in positions 3, 4, and 5, in turn, effectuates equal inhibition of HDAC1 and HDAC6 or a marginal preference for the latter. The HDAC6 selectivity achieved by appropriate R² residues may moreover be boosted by choosing the *tert*-butyl motif over a cyclohexyl group in position R¹. Overall, all new ligands, except for the most selective inhibitor **10p**, outmatched the HDAC6 inhibition of the control compound vorinostat and were equally potent as tubastatin A and ricolinostat.

The comparison of the unselective inhibitors **10a** and **10h** with their non-fluorinated analogs DDK115 and DDK137 implies that linker fluorination results in decreased HDAC1 inhibition (DDK115 vs. **10a**: 0.249 μM/0.310 μM; DDK137 vs. **10h**: 0.005 μM/0.013 μM) accompanied by higher or similar inhibitory activity against HDAC6 (DDK115 vs. **10a**:

0.040 μM /0.020 μM ; DDK137 vs. **10h**: 0.011 μM /0.010 μM), thus almost tripling the selectivity for HDAC6 in both cases.

In respect of the HDAC6-selective compounds **IIe** and **IIf**, linker fluorination increased the inhibitory activity toward HDAC1 (**IIe** vs. **10l**: 2.41 μM /1.75 μM ; **IIf** vs. **10m**: 3.11 μM /1.75 μM) and nearly doubled inhibitory potency against HDAC6 (**IIe** vs. **10l**: 0.051 μM /0.027 μM ; **IIf** vs. **10m**: 0.038 μM /0.017 μM), thereby improving the selectivity profiles.

Those results are generally in line with the observations reported by Sandrone *et al.* who concluded that the increased HDAC6 selectivity of HDACi with mono- or difluorinated linkers in *meta*-position to the hydroxamic acid results from increased HDAC6 inhibition and/or decreased inhibitory activity toward HDAC1.⁴⁷ Differences in the assay setups (in particular different substrates) prohibit a direct comparison of the results published by Sandrone *et al.* and our results summarized in Table 1 so that we chose to include givinostat as an additional control compound. Although we (IC₅₀ HDAC1: 0.035 μM ; HDAC6: 0.014 μM , SI: 2.5) measured different IC₅₀ values for givinostat compared to Sandrone *et al.* (IC₅₀ HDAC1: 0.070 μM ; HDAC6: 0.023 μM , SI: 3)⁴⁷, the resulting selectivity indices were comparable (Table 1). In general, Sandrone *et al.* observed different reasons for the increased HDAC6 selectivity depending on whether small cap-less inhibitors or more complex larger HDACi with (hetero)aromatic caps were investigated. In the case of small cap-less HDACi, the increased HDAC6 selectivity is mainly driven by improved HDAC6 inhibition. This was exemplified by the comparison of *N*-hydroxybenzamide (IC₅₀ HDAC1: 25.4 μM ; HDAC6: 1.34 μM , SI: 19) and 3-fluoro-*N*-hydroxybenzamide (IC₅₀ HDAC1: 29.4 μM ; HDAC6: 0.453 μM , SI: 65).⁴⁷ The improvement of the HDAC6 selectivity of larger HDACi with complex (hetero)aromatic caps, in contrast, originates mainly from a decreased HDAC1 inhibition.⁴⁷ This can be explained by differences in the L1 loops of HDAC1 and HDAC6: the active site of HDAC1 is more restricted and thus unable to accommodate larger cap groups, whereas HDAC6 features a wider entrance area to the catalytic tunnel.⁴⁷ Moreover, unlike most other HDACs which feature an aspartate in the respective position, HDAC6 possesses a serine (Ser531) on loop L2 at the entrance of the catalytic channel.⁴⁷ In the case of larger HDACi with (hetero)aromatic caps, a fluorine atom in *meta*-position of the linker is oriented toward loop L2 which might result in a steric repulsion in HDACs featuring an aspartate at the tunnel entrance. This could explain the results observed by Sandrone *et al.*, indicating that fluorinated phenyl linkers with a bulky cap group are more likely to reduce the inhibitory activity toward HDAC1 rather than increasing the potency against HDAC6, thus boosting the selectivity.⁴⁷ Considering our data and the results published by Sandrone *et al.*⁴⁷, it can be concluded that linker fluorination has a distinct beneficial effect on HDAC6 inhibition and/or selectivity.

In addition to the above-mentioned effects on HDAC6, Sandrone *et al.*⁴⁷ found that the linker fluorination restores activity against class IIa HDACs. To investigate whether this is also the case for our peptoid-based HDACi, we screened DDK137, the direct non-fluorinated analogue of compound **10h**, against HDAC4. In good agreement with the results of Sandrone *et al.*⁴⁷, DDK137 (IC₅₀ HDAC4: 2.67 μM) demonstrated reduced HDAC4 inhibition compared to **10h** (IC₅₀ HDAC4: 1.88 μM , Figure 1), thus indicating that linker fluorination can lead to improved inhibitory properties against class IIa HDACs.

Crystal Structure of HDAC6 in Complex with 10h.

The 1.85 Å-resolution structure of the HDAC6-**10h** complex contains four independent copies of the enzyme-inhibitor complex in the asymmetric unit of the crystal. Hydroxamate-Zn²⁺ coordination differs in each of the four structures. In chain A, hydroxamate-Zn²⁺ coordination is modeled with bidentate geometry but the electron density for the hydroxamate group is ambiguous. In chains B and C, exclusively bidentate hydroxamate-Zn²⁺ coordination geometry is observed, and in chain D exclusively monodentate hydroxamate-Zn²⁺ coordination geometry is observed. Below, the structures of the enzyme-inhibitor complex in chain B and chain D are outlined in greater detail.

For chain B (Figure 2), the HDAC6-**10h** complex does not reveal any major structural rearrangements caused by inhibitor binding, and the root-mean-square deviation (rmsd) is 0.19 Å for 311 Ca atoms between the inhibitor-bound and unliganded enzyme structures. In the bidentate hydroxamate-Zn²⁺ chelate complex, the Zn²⁺-O distances are 2.2 and 2.3 Å for the N-O⁻ and C=O groups, respectively. The side chain of Y745 additionally donates a hydrogen bond to the hydroxamate C=O group (O-O distance = 2.6 Å) and H574 accepts a hydrogen bond from the hydroxamate NH group (N-N distance = 2.8 Å).

The fluorophenyl linker is nestled in the aromatic crevice formed by F583 and F643; however, the aromatic ring adopts two mutually exclusive conformations (50% occupancy each). In one conformation, the C-F group is oriented into the crevice and the fluorine atom is 3.4 Å away from the hydroxyl group of S531. In the other conformation, the C-F group is oriented toward solvent. The peptoid carbonyl group is oriented toward solvent and appears to form an *n*→*π** interaction with the adjacent benzylamide carbonyl group. The dimethylaniline group resides in the L1 loop pocket, as observed for the non-fluorinated inhibitor.⁴⁵ The benzylamide carbonyl forms hydrogen bonds with bulk solvent, while the adjacent nitrogen forms a water mediated hydrogen bond with the hydroxyl side chain of S531.

For chain D (Figure 3), the HDAC6-**10h** complex does not reveal any major structural rearrangements caused by inhibitor binding, and the rmsd is 0.16 Å for 302 Ca atoms between the inhibitor-bound and unliganded enzyme structures. The hydroxamate moiety adopts monodentate Zn²⁺ coordination geometry in which the hydroxamate N-O⁻ group coordinates to Zn²⁺ at a distance of 1.8 Å. The hydroxamate C=O group accepts a short hydrogen bond from the Zn²⁺-coordinated water molecule (O-O distance = 2.3 Å) which in turn forms hydrogen bonds with H573 and H574. The hydroxamate NH group additionally interacts with the side chain of Y745 (O-N distance = 2.5 Å).

The fluorophenyl aromatic linker is nestled in the F583-F643 aromatic crevice with the C-F group oriented exclusively into the crevice; the fluorine atom is 3.4 Å away from the hydroxyl group of S531. Other aspects of inhibitor binding are similar to those observed in chain B described above. The peptoid carbonyl of the inhibitor capping group is oriented toward solvent and the carbonyl oxygen appears to form an *n*→*π** interaction with the adjacent benzylamide carbonyl group. The benzylamide carbonyl and peptoid carbonyl form a hydrogen bond network with four water molecules, and this network includes Zn²⁺ ligand H614. The benzylamide NH group forms a water mediated hydrogen bond with the side

chain of S531. Finally, the dimethylaniline group resides in the L1 loop pocket. The overall binding modes of **10h** and its non-fluorinated counterpart⁴⁴ are almost entirely identical, with the only major difference being variations in hydroxamate-Zn²⁺ coordination (Figure 4).

Bavarostat is a selective inhibitor of HDAC6⁴⁴ and contains a *meta*-fluorophenyl linker that, like the *meta*-fluoro linker of **10h**, binds in the aromatic crevice defined by F583 and F643.⁴⁵ More recently, inhibitors have been developed that contain *meta*-fluorophenyl and *meta*-difluorophenyl linkers with different capping groups, and these inhibitors exhibit enhanced selectivity for inhibition of HDAC6 over HDAC1.⁴⁷ The X-ray crystal structure of one of these inhibitors complexed with HDAC6 reveals that the *meta*-difluorophenyl linker makes favorable π - π interactions in the aromatic crevice as well as weak interaction between one of the C-F groups and S531. The fluoroaromatic ring of this inhibitor generally binds in a similar manner to the fluoroaromatic rings of bavarostat and **10h**, although the inhibitor binding orientation is slightly tilted so that the rings are not coplanar (Figure 4b). Intriguingly, a key feature of isozyme selectivity derives from the reduction of inhibitory potency toward HDAC1, especially for inhibitors containing a *meta*-difluorophenyl linker.

Cytotoxic effects on leukemia cell lines.

The sixteen new inhibitors (**10a–10p**) were screened against three-selected leukemia cell lines originated from myeloid (HL60), B- (HAL01) or T- (Jurkat) lymphoid lineages (Table 2). The FDA-approved drug vorinostat, the HDAC6i HPOB, and the clinical candidate ricolinostat were used as controls. For selective HDAC6i, cytotoxicity levels are typically low and therefore, it was not surprising that neither of the IC₅₀ values measured in presence of selective ligands lies below the micromolar concentration range.^{29,54} Compound **10j** was found to resemble ricolinostat in terms of both HDAC inhibition and isoform selectivity. Accordingly, it induced similar levels of cytotoxicity with IC₅₀ values ranging from 1.46 μ M to 2.47 μ M in all three cell lines. Two other compounds, **10c** and **10d**, exceeded the cytotoxic effects of HPOB throughout all screenings. As for the unselective inhibitors, the most potent derivative **10h** proved to be similarly active against the B-cell acute lymphoblastic leukemia (B-ALL) cell line HAL01 and even more toxic against the T-ALL Jurkat cell line than vorinostat. Based on these results, compound **10h** was picked as the most promising candidate for additional experiments.

Extended functional analysis of **10h** in leukemia cell lines.

To study the inhibitory effects of the hit compound **10h** (with highest cytotoxicity) on the growth and apoptosis induction of leukemia cells, further functional assays were carried out. First, we evaluated the effects of **10h** and on the cellular viability of a broad range of leukemia cell lines originated from therapy refractory subgroups; the class I selective HDACi CI994 (tacedinaline; phase III) and the HDAC6i ricolinostat were used as controls (Figure 5A and Supplementary Table S1, Supporting Information). In order to exclude the general cytotoxicity effects (i.e. therapeutic window) of **10h** exposure, two healthy human fibroblast controls were also included in the assays. **10h** markedly outperformed CI994 and ricolinostat in inhibiting the cellular viability of most tested leukemia cell lines at a much lower IC₅₀ concentration range than the healthy fibroblast controls (Supplementary

Table S1, Supporting Information). Next, the induction of apoptosis following the treatment of HL60 cells with 1 μM or 5 μM of **10h** (for 48 h) was determined (Figure 5B). The treated cells were stained with annexin V and propidium iodide to be analyzed by flow cytometry. The significant ($p < 0.0001$) increase in apoptotic cells observed upon treatment with **10h** at 1 μM as well as 5 μM indicates that induction of apoptosis contributes to its antiproliferative potential. To further determine the intracellular target specificity of **10h**, HL60 cells were treated with the respective $\text{IC}_{12.5}$, IC_{25} , IC_{50} , and IC_{75} concentrations of **10h** and subsequently immunoblotted along with the reference HDAC6i ricolinostat at its IC_{50} concentration (Figure 5C). After incubation with **10h**, a dose-dependent increase in the acetylation of α -tubulin and histone 3 (H3) was observed. As expected, ricolinostat-treated cells showed prominent acetylation of α -tubulin and lower Ac-H3 levels than observed for **10h**.

Resistance against single use of HDACi is often reported,^{55,56} however, co-administration of HDACi with either chemotherapeutic agents or targeted drugs can maximize their efficacy by minimizing the resistance development incidences and through reducing the toxicity by lowering the doses. We have previously shown the synergistic effects of HDACi in combination with proteasome inhibitors.^{49,57,58,59} In the present study, we focused on finding clinically relevant synergistic partners of HDACi which are frequently used in the therapy protocol for the treatment of leukemia. For instance, in previous preclinical reports, the combination of DNA hypomethylating agents along with HDACi was reported to be synergistic in different hematological malignancies, potentially by disrupting the transcriptional repressor complex involving methyl-CpG binding proteins and HDACs.^{31,60,61} Therefore, we evaluated the synergistic effects of **10h** in combination with decitabine, a DNA methyl transferase inhibitor (DNMTi) used to treat myelodysplastic syndromes (Figure 6A). Interestingly, the combination of **10h** and decitabine was found differentially synergistic in the tested myeloid lineage-derived cell lines HL60 (ZIP synergy score: 25.08) and MOLM13 (27.44) but not in the tested B- or T-lymphoid-lineage-originated leukemic cell lines HAL01 (1.18) and Jurkat (-0.87), respectively (Figure 6A). The observed synergism of **10h** with decitabine later prompted us to examine the underlying molecular mechanism. The co-administration of **10h** and decitabine revealed a strong induction of acetylation of H3 as compared to mono-treatment, thus indicating that class I HDAC inhibition is required for the synergistic activity with decitabine and the resulting enhancement of anticancer activity (Figure 6B).

Extended functional analysis of **10p** in leukemia cell lines.

In parallel the inhibitory effects the most selective HDAC6i **10p** on the leukemia cell growth and apoptosis induction were determined. As expected, **10p** had a significantly weaker impact on the viability of tested leukemia cell lines, with IC_{50} values ranging in the high micromolar concentration (Figure 5A and Supplementary Table S1, Supporting Information). Similarly in the apoptosis assay, which was performed after treatment of HL60 cells with the 1 μM or 5 μM of **10p** for 48h, a weaker (in comparison to **10h**) although significant ($p < 0.05$) apoptosis induction was noticed (Figure 5B). Furthermore, in order to evaluate the intracellular specificity of **10p**, HL60 cells were treated with the respective $\text{IC}_{12.5}$, IC_{25} , IC_{50} , and IC_{75} concentrations of **10p** and immunoblotted along

with the reference HDAC6i ricolinostat at its IC₅₀ concentration. In agreement, treatment with a selective HDAC6i **10p** induced acetylation of α -tubulin, but had no effect on Ac-H3 levels even at concentrations of up to 36 μ M (Figure 5C). In a similar manner, we next analyzed the combinatorial potential of **10p** in combination with decitabine, which revealed a moderate (in comparison to **10h**) synergism in the tested AML cell lines HL60 (7.78) and MOLM13 (7.18) (Figure 7).

Overall, these data support the therapeutic potential of **10h** and **10p** in leukemia, especially for AML when used in combination with decitabine.

CONCLUSIONS

Selected from a library of sixteen compounds that were synthesized using a simple, microwave-assisted 2-step protocol, **10h** stood out due to its notable antileukemic effects and, importantly, with low cytotoxic activity toward healthy cells. Additional drug combinatorial drug screenings demonstrated a strong synergistic interaction of **10h** with decitabine, which was especially prominent against AML cells. Designed as a pan-inhibitor, **10h** proved potent inhibition of class I HDACs and HDAC6 in biochemical and cellular assays. The analysis of a crystal structure of the CD2 from zebrafish HDAC6 complexed with **10h** disclosed differences in the zinc coordination but similar occupation of the L1 loop pocket in comparison to its non-fluorinated analog. The remarkable HDAC6 selectivity of our other hit compound **10p** outmatched tubastatin A in biochemical enzyme inhibition assays and was confirmed in western blotting experiments. Despite moderate cytotoxicity on its own, the combination of **10p** and decitabine displayed moderate synergism in AML cell lines, thus indicating the potential of **10p** for combination therapies and targeted therapies involving HDAC6i. On the whole, our study provided valuable SAR data that can be used to fine-tune selectivity profiles toward HDAC6i or unselective, but highly cytotoxic pan-HDACi.

EXPERIMENTAL SECTION

Chemistry.

Dry MeOH was obtained from the MBraun MB SPS-800 solvent purification system. Except for DCM, which was purified by distillation prior to use, all reagents and solvents were purchased from commercial sources and used without further purification. Thin layer chromatography was carried out using Macherey-Nagel pre-coated aluminium foil sheets, which were visualized using UV light (254 nm). Hydroxamic acids were further stained using a 1% solution of iron(III) chloride in MeOH. ¹H-NMR and ¹³C-NMR spectra were recorded at rt or, due to the occurrence of rotamers, at 60 °C using Bruker Avance III HD (400 MHz), and Varian/Agilent Mercury-plus (300 MHz & 400 MHz) spectrometers. Chemical shifts (δ) are quoted in parts per million (ppm). All spectra were standardized in accordance with the signals of the deuterated solvents (DMSO-*d*₆: δ_{H} = 2.50 ppm; δ_{C} = 39.5 ppm; CDCl₃: δ_{H} = 7.26 ppm; δ_{C} = 77.0 ppm). Coupling constants (J) are reported in Hertz (Hz). Mass-spectra were measured by the Leipzig University Mass Spectrometry Service via electrospray ionization (ESI) on Bruker Daltonics Impact II and Bruker Daltonics micrOTOF spectrometers. The uncorrected melting points were determined using

a Barnstead Electrothermal 9100 apparatus. Analytical HPLC analysis were carried out using a Thermo Fisher Scientific UltiMate 3000 system equipped with an UltiMate™ HPG-3400SD pump, an UltiMate™ 3000 Diode array detector, an UltiMate™ 3000 autosampler, and a TCC-3000SD standard thermostatted column compartment by Dionex. The system was operated using a Macherey-Nagel NUCLEODUR 100–5 C₁₈ ec column (250 mm x 4.6 mm). UV absorption was detected at 254 nm with a linear gradient of 5% B to 95% B within 23 min. HPLC-grade water + 0.1% TFA (solvent A) and HPLC-grade acetonitrile + 0.1% TFA (solvent B) were used for elution at a flow rate of 1 mL/min. The purity of the final compounds was at least 95.0%.

Methyl 3-fluoro-4-methylbenzoate (2).

To a cooled (0 °C) solution of 3-fluoro-4-methylbenzoic acid (5.00 g, 32.5 mmol, 1.0 eq) in MeOH (150 mL) was added thionyl chloride (3.05 mL, 42.5 mmol, 1.3 eq) and the resulting mixture was stirred at rt for 16 h. Upon removal of the solvent under reduced pressure, the residue was dissolved in EtOAc (200 mL) and 10% HCl (50 mL) was added. The mixture was extracted with EtOAc (3 x 100 mL) and the combined organics were washed with sat. aq. NaHCO₃ (2 x 20 mL) and water (1 x 20 mL). Drying over MgSO₄ and evaporation of the solvent afforded **2** as a pale yellow liquid (5.10 g, 30.4 mmol, 93%). Spectroscopic data matched those reported in the literature.⁶³

Methyl 4-(bromomethyl)-3-fluorobenzoate (3).

Synthesized according to the procedure reported in the literature.⁵⁰ To a solution of **2** (4.91 g, 29.0 mmol, 1.0 eq) and NBS (7.83 g, 44.0 mmol, 1.5 eq) in DCM (150 mL) was added AIBN (476 mg, 2.90 mmol, 0.1 eq). The mixture was first refluxed for 10 h and then stirred at rt for another 16 h after which DCM (100 mL) was added. The resulting solution was washed with 1M NaOH (3 x 50 mL) and brine (2 x 50 mL) before it was dried over Na₂SO₄. Removal of the solvent under reduced pressure afforded the crude product **3** (quant.) as a colourless liquid that solidified upon storage at –18 °C. The crude product was used without further purification.

Methyl 4-(aminomethyl)-3-fluorobenzoate hydrochloride (5).

This compound was synthesized according to the procedure reported in the literature.⁵⁰ A solution of **3** (1.62 g, 6.50 mmol, 1.0 eq) and NaN₃ (510 mg, 7.80 mmol, 1.2 eq) in DMF (25 mL) was stirred at 80 °C for 12 h. After cooling to rt, brine (25 mL) was added and the resulting solution was extracted with a mixture of Et₂O and cyclohexane (1:1; 3 x 100 mL). The combined organics were washed with brine (2 x 20 mL), dried over MgSO₄ and concentrated under reduced pressure to afford **4** as a pale yellow liquid. The crude azide thus obtained was subsequently dissolved in a mixture of THF (40 mL) and water (4 mL) to which triphenylphosphine (3.00 g, 11.4 mmol, 1.8 eq) was added in small portions. After stirring at rt for 40 h, the solvent was evaporated. The residue was redissolved in DCM (200 mL) and extracted with 4M HCl (2 x 50 mL). The combined aqueous layers were then basified using 2M NaOH (pH 10) and extracted with DCM (3 x 100 mL). Drying of the combined organics over MgSO₄ and removal of the solvent under reduced pressure afforded the crude amine which was precipitated from MeOH (2 mL), 37% HCl (0.5 mL), and Et₂O

(20 mL) to afford the hydrochloride salt **5** as a white solid (553 mg, 2.50 mmol, 39% over 2 steps); mp 236–241 °C; ¹H NMR (400 MHz, DMSO-*d*₆): δ 8.70 (s, 3H, NH₃⁺), 7.87–7.62 (m, 3H, arom.), 4.12 (q, *J* = 5.8 Hz, 2H, CH₂), 3.88 (s, 3H, OCH₃) ppm; ¹³C NMR (101 MHz, DMSO-*d*₆): δ 164.9, 161.2, 158.7, 132.0, 131.9, 131.7, 131.6, 126.6, 126.5, 125.2, 125.1, 115.9, 115.7, 52.6, 35.4 ppm; HRMS (*m/z*): MNa⁺ calcd for C₉H₁₀FNO₂ 184.0768, found 184.0771.

General procedure A.

The linker building block **5** (132 mg, 0.60 mmol, 1.2 eq), paraformaldehyde (18.0 mg, 0.60 mmol, 1.2 eq), and crushed molecular sieves 4 Å (50.0 mg) were suspended in MeOH (1.0 mL) and Et₃N (0.08 mL, 0.60 mmol, 1.2 eq) was added. The mixture was subjected to microwave irradiation at 150 W and 45 °C for 20 min before the respective isonitrile (0.50 mmol, 1.0 eq) and the respective carboxylic acid (0.50 mmol, 1.0 eq) were added. The resulting mixture was again subjected to microwave irradiation at the same settings for 60 min after which the molecular sieves were removed by filtration and washed with DCM (10 mL). The filtrate was concentrated under reduced pressure and the residue was redissolved in DCM (100 mL), washed with 10% HCl (1 x 10 mL), water (1 x 10 mL), 1M NaOH (2 x 5 mL), and brine (1 x 10 mL). The organic layer was dried over MgSO₄ and the solvent was removed under reduced pressure to afford the crude product **9** which was recrystallized from EtOAc (1 mL) and petrol (20 mL). The ester thus obtained was allowed to dry before it was added to a mixture of NaOH (200 mg, 5.00 mmol, 10 eq) and hydroxylamine (50% solution in water; 0.95 mL, 15.5 mmol, 31 eq) in MeOH (4 mL) and DCM (1 mL). The resulting solution was stirred at 0 °C for approx. 15 min until TLC (DCM/MeOH 9:1) indicated full conversion upon which the solvents were evaporated and the residue was dissolved in water (10 mL). Dropwise addition of 10% HCl (pH 8) induced precipitation of the hydroxamic acid **10** which was then isolated by filtration and washed with 5% HCl (2 x 3 mL) and chilled water (3 x 5 mL), successively. For compounds derived from *tert*-butyl isocyanide, precipitation of the product was often incomplete so that the aqueous layer was further extracted with EtOAc (3 x 30 mL). The combined organics were washed with brine (1 x 10 mL) and dried over Na₂SO₄. Removal of the solvent under reduced pressure yielded the remaining product.

General procedure B.

The linker building block **5** (109 mg, 0.50 mmol, 1.0 eq), paraformaldehyde (15.0 mg, 0.50 mmol, 1.0 eq), and crushed molecular sieves 4 Å (50.0 mg) were suspended in MeOH (1.0 mL) and Et₃N (0.08 mL, 0.60 mmol, 1.2 eq) was added. The mixture was subjected to microwave irradiation at 150 W and 45 °C for 30 min before the respective isonitrile (0.50 mmol, 1.0 eq) and 4-(dimethylamino)benzoic acid (83.0 mg, 0.50 mmol, 1.0 eq) were added. The resulting mixture was again subjected to microwave irradiation at the same settings for 3 h after which the molecular sieves were removed by filtration and washed with DCM (10 mL). The filtrate was concentrated under reduced pressure and the residue was redissolved in DCM (100 mL) and washed with 1M NaOH (2 x 5 mL), water (1 x 10 mL), and brine (1 x 10 mL). Drying over MgSO₄ and evaporation of the solvent afforded the crude product **9** which was recrystallized from EtOAc (1 mL) and petrol (20 mL). The ester thus obtained was allowed to dry before it was added to a mixture of NaOH (200 mg, 5.00 mmol, 10

eq) and hydroxylamine (50% solution in water; 0.95 mL, 15.5 mmol, 31 eq) in MeOH (4 mL) and DCM (1 mL). The resulting solution was stirred at 0 °C for approx. 15 min until TLC (DCM/MeOH 9:1) indicated full conversion. The organic solvents were removed under reduced pressure and the residue was dissolved in water (10 mL). Dropwise addition of 10% HCl (pH 8) induced precipitation of the hydroxamic acid **10** which was then isolated by filtration and washed with chilled water (3 x 5 mL). For compound **10j** derived from *tert*-butyl isocyanide, precipitation of the product was incomplete so that the aqueous layer was extracted with EtOAc (3 x 30 mL). The combined organics were washed with brine (1 x 10 mL) and dried over Na₂SO₄. Removal of the solvent under reduced pressure yielded the remaining product.

4-({*N*-[(Cyclohexylcarbamoyl)methyl]-1-(3,5-dimethylphenyl)formamido}methyl)-3-fluoro-*N*-hydroxybenzamide (**10a**).

Synthesis according to general procedure A using 3,5-dimethylbenzoic acid (75.0 mg) and cyclohexyl isocyanide (0.06 mL) afforded **10a** as a white solid (86.0 mg, 0.18 mmol, 38%); mp 177 °C; t_R : 8.02 min, purity: 99.7%; ¹H NMR (400 MHz, DMSO-*d*₆, 20 °C): δ 7.75 (d, *J* = 8.2 Hz, 1H, NH), 7.63–7.31 (m, 3H, arom.), 7.10–6.93 (m, 3H, arom.), 4.68/4.52 (2 x s, 2H, CH₂), 3.91/3.72 (2 x s, 2H, CH₂), 3.52 (s, 1H, CH), 2.26/1.80 (2 x s, 6H, 2 x CH₃), 1.74–0.97 (m, 10H, c-Hexyl) ppm; ¹³C NMR (101 MHz, DMSO-*d*₆): δ 171.6, 166.7, 162.4, 161.3, 158.9, 137.6, 135.9, 130.9, 129.8, 124.1, 122.9, 113.7, 113.4, 51.4, 47.7, 43.0, 32.4, 32.3, 25.2, 24.4, 20.8 ppm; HRMS (m/z): MNa⁺ calcd for C₂₅H₃₀FN₃O₄ 478.2113, found 478.2128.

4-({*N*-[(Cyclohexylcarbamoyl)methyl]-1-[4-(dimethylamino)phenyl]formamido}methyl)-3-fluoro-*N*-hydroxybenzamide (**10b**).

Synthesis according to general procedure B using cyclohexyl isocyanide (0.06 mL) afforded **10b** as a white solid (162 mg, 0.34 mmol, 69%); mp 123 °C; t_R : 6.38 min, purity: 98.1%; ¹H NMR (400 MHz, DMSO-*d*₆, 20 °C): δ 11.31 (s, 1H, *NH*-OH), 9.17 (s, 1H, OH), 7.81 (s, 1H, NH), 7.70–7.26 (m, 5H, arom.), 6.78–6.62 (m, 2H, arom.), 4.64 (s, 2H, CH₂), 3.85 (s, 2H, CH₂), 3.55 (d, *J* = 9.8 Hz, 1H, CH), 2.93 (s, 6H, 2 x CH₃), 1.76–1.45 (m, 5H, c-Hexyl), 1.31–1.02 (m, c, 5H-Hexyl) ppm; ¹³C NMR (101 MHz, DMSO-*d*₆): δ 171.7, 166.9, 162.5, 161.2, 158.9, 151.3, 133.9, 129.8, 128.7, 127.5, 127.4, 123.0, 121.9, 113.7, 113.5, 111.0, 47.6, 32.3, 25.2, 24.5 ppm; HRMS (m/z): MNa⁺ calcd for C₂₅H₃₁FN₄O₄ 493.2222, found 493.2214.

4-({*N*-[(Cyclohexylcarbamoyl)methyl]-1-(2-fluorophenyl)formamido}methyl)-3-fluoro-*N*-hydroxybenzamide (**10c**).

Synthesis according to general procedure A using 2-fluorobenzoic acid (70.0 mg) and cyclohexyl isocyanide (0.06 mL) afforded **10c** as a pink solid (85.0 mg, 0.19 mmol, 38%); mp 179 °C; t_R : 7.40 min, purity: 96.6%; ¹H NMR (300 MHz, DMSO-*d*₆, 20 °C): δ 11.30 (d, *J* = 4.7 Hz, 1H, *NH*-OH), 9.14 (s, 1H, OH), 7.77–7.16 (m, 8H, arom., NH), 4.73/4.50 (2 x s, 2H, CH₂), 3.98/3.73 (2 x s, 2H, CH₂), 3.47–3.40 (m, 1H, CH), 1.81–1.43 (m, 5H, c-Hexyl), 1.36–0.89 (m, 5H, c-Hexyl) ppm; ¹³C NMR (101 MHz, DMSO-*d*₆): δ 166.5, 166.0, 165.9, 162.6, 161.3, 161.1, 158.9, 158.8, 158.7, 156.5, 156.3, 133.9, 131.5, 131.4, 129.8, 129.7,

129.6, 128.72, 128.68, 128.4, 127.1, 126.9, 124.8, 124.7, 124.6, 124.0, 123.8, 122.9, 115.9, 115.7, 113.9, 113.6, 50.9, 47.62, 47.55, 47.1, 47.0, 43.2, 32.4, 32.1, 25.2, 25.1, 24.5, 24.3 ppm; HRMS (m/z): M^- calcd for $C_{23}H_{25}F_2N_3O_4$ 444.1740, found 444.1741.

4-({N-[(Cyclohexylcarbamoyl)methyl]-1-(2-methylphenyl)formamido)methyl}-3-fluoro-N-hydroxybenzamide (10d).

Synthesis according to general procedure A using 2-methylbenzoic acid (68.0 mg) and cyclohexyl isocyanide (0.06 mL) afforded **10d** as a pink solid (84.0 mg, 0.19 mmol, 38%); mp 115 °C; t_R : 7.55 min, purity: 95.1%; 1H NMR (400 MHz, DMSO- d_6 , 60 °C): δ 11.12 (s, 1H, *NH*-OH), 8.99 (s, 1H, OH), 7.71–7.37 (m, 4H, arom., NH), 7.37–7.06 (m, 4H, arom.), 4.75/4.41 (2 x s, 2H, CH₂), 4.01/3.64 (2 x s, 2H, CH₂), 3.48 (d, J = 9.7 Hz, 1H, CH), 2.30/2.22 (2 x s, 3H, CH₃), 1.82–1.47 (m, 5H, c-Hexyl), 1.36–0.95 (m, 5H, c-Hexyl) ppm; ^{13}C NMR (75 MHz, DMSO- d_6): δ 171.1, 166.2, 135.8, 134.3, 134.1, 130.3, 128.8, 125.7, 125.6, 123.0, 113.9, 113.6, 50.6, 47.7, 47.6, 42.5, 40.1, 32.4, 32.2, 25.2, 25.1, 24.5, 24.4, 18.5 ppm; HRMS (m/z): M^- calcd for $C_{24}H_{28}FN_3O_4$ 440.1991, found 440.1988.

4-({N-[(Cyclohexylcarbamoyl)methyl]-1-(2-methoxyphenyl)formamido)methyl}-3-fluoro-N-hydroxybenzamide (10e).

Synthesis according to general procedure A using 2-methoxybenzoic acid (76.0 mg) and cyclohexyl isocyanide (0.06 mL) afforded **10e** as a white solid (121 mg, 0.26 mmol, 53%); mp 130 °C; t_R : 7.33 min, purity: 95.1%; 1H NMR (400 MHz, DMSO- d_6 , 20 °C): δ 11.31 (d, J = 6.8 Hz, 1H, *NH*-OH), 9.14 (s, 1H, OH), 7.69–6.92 (m, 8H, arom. NH), 4.95 (s, 1H, CH₂), 4.46–3.99 (m, 2H, CH₂), 3.83–3.57 (m, 4H, OCH₃, CH₂), 3.47–3.39 (m, 1H, CH), 1.80–1.43 (m, 5H, c-Hexyl), 1.32–0.90 (m, 5H, c-Hexyl) ppm; ^{13}C NMR (75 MHz, DMSO- d_6): δ 169.2, 169.1, 166.3, 166.2, 162.7, 161.6, 158.3, 154.9, 154.5, 133.61, 130.57, 130.4, 129.0, 127.7, 125.3, 125.1, 123.0, 120.5, 113.7, 113.4, 111.4, 55.6, 55.3, 50.7, 47.5, 42.7, 32.4, 32.2, 25.1, 24.5, 24.4 ppm; HRMS (m/z): MH^+ calcd for $C_{24}H_{28}FN_3O_5$ 458.2086, found 458.2066.

4-({N-[(Cyclohexylcarbamoyl)methyl]-1-[2-(trifluoromethyl)phenyl]formamido)methyl}-3-fluoro-N-hydroxybenzamide (10f).

Synthesis according to general procedure A using 2-(trifluoromethyl)benzoic acid (95.0 mg) and cyclohexyl isocyanide (0.06 mL) afforded **10f** as a white solid (142 mg, 0.29 mmol, 57%); mp 107 °C; t_R : 7.84 min, purity: 95.0%; 1H NMR (400 MHz, DMSO- d_6 , 20 °C): δ 11.31 (d, J = 8.4 Hz, 1H, *NH*-OH), 9.15 (s, 1H, OH), 7.95–7.23 (m, 8H, arom., NH), 5.27–5.07/4.60–4.24 (2 x m, 2H, CH₂), 3.70–3.43 (m, 3H, CH, CH₂), 1.81–1.43 (m, 5H, c-Hexyl), 1.36–0.91 (m, 5H, c-Hexyl) ppm; ^{13}C NMR (101 MHz, DMSO- d_6): δ 168.6, 168.5, 166.0, 162.5, 161.4, 159.0, 158.7, 134.2, 134.1, 134.0, 132.7, 132.0, 131.5, 131.4, 130.5, 130.0, 129.8, 129.7, 128.8, 128.7, 127.6, 126.7, 126.54, 126.49, 126.45, 125.5, 125.2, 125.0, 124.9, 122.8, 122.3, 113.8, 113.6, 50.6, 47.7, 47.5, 47.0, 42.5, 32.4, 32.1, 25.2, 25.1, 24.5, 24.3 ppm; HRMS (m/z): M^- calcd for $C_{24}H_{25}F_4N_3O_4$ 494.1708, found 494.1718.

4-({*N*-[(Benzylcarbamoyl)methyl]-1-(3,5-dimethylphenyl)formamido}methyl)-3-fluoro-*N*-hydroxybenzamide (10g).

Synthesis according to general procedure A using 3,5-dimethylbenzoic acid (75.0 mg) and benzyl isocyanide (0.06 mL) afforded **10g** as a dark brown solid (85.0 mg, 0.18 mmol, 37%); mp 215 °C; t_R : 7.77 min, purity: 95.2%; 1H NMR (300 MHz, DMSO- d_6 , 20 °C): δ 11.31 (s, 1H, *NH*-OH), 9.14 (s, 1H, OH), 8.42 (s, 1H, NH), 7.75–6.92 (m, 11H, arom.), 4.71/4.59 (s, 2H, CH₂), 4.36–4.23 (m, 2H, CH₂), 4.02/3.87 (s, 2H, CH₂), 2.24 (s, 6H, 2 x CH₃) ppm; ^{13}C NMR (101 MHz, DMSO- d_6): δ 171.6, 167.8, 139.4, 139.3, 139.1, 139.0, 137.6, 136.1, 135.8, 131.1, 130.9, 129.9, 129.8, 129.6, 129.51, 129.45, 128.3, 127.2, 126.9, 124.1, 123.1, 123.0, 113.9, 113.7, 51.5, 43.1, 42.2, 20.8 ppm; HRMS (m/z): M^- calcd for C₂₆H₂₆FN₃O₄ 462.1835, found 462.1839.

4-({*N*-[(Benzylcarbamoyl)methyl]-1-[4-(dimethylamino)phenyl]formamido}methyl)-3-fluoro-*N*-hydroxybenzamide (10h).

Synthesized according to general procedure B using benzyl isocyanide (0.06 mL). The reaction time for the ester formation was reduced to 60 min (imine formation: 20 min, U4CR: 40 min). **10h** was obtained as an off-white solid (162 mg, 0.34 mmol, 68%); mp 205 °C; t_R : 6.35 min, purity: 97.2%; 1H NMR (400 MHz, DMSO- d_6 , 20 °C): δ 11.31 (s, 1H, *NH*-OH), 9.16 (s, 1H, OH), 8.47 (t, J = 6.0 Hz, 1H, NH), 7.68–7.43 (m, 3H, arom.), 7.39–7.16 (m, 7H, arom.), 6.74–6.58 (m, 2H, arom.), 4.69 (s, 2H, CH₂), 4.30 (d, J = 5.8 Hz, 2H, CH₂), 3.96 (s, 2H, CH₂), 2.93 (s, 6H, NMe₂) ppm; ^{13}C NMR (101 MHz, DMSO- d_6): δ 171.8, 168.2, 162.5, 158.7, 151.3, 139.2, 133.8, 128.6, 128.3, 127.2, 126.8, 123.0, 113.8, 110.9, 42.1 ppm; HRMS (m/z): MNa^+ calcd for C₂₆H₂₇FN₄O₄ 501.1909, found 501.1910.

4-({*N*-[(*tert*-Butylcarbamoyl)methyl]-1-(3,5-dimethylphenyl)formamido}methyl)-3-fluoro-*N*-hydroxybenzamide (10i).

Synthesis according to general procedure A using 3,5-dimethylbenzoic acid (75.0 mg) and *tert*-butyl isocyanide (0.06 mL) afforded **10i** as a white solid (125 mg, 0.29 mmol, 58%); mp 162 °C; t_R : 7.72 min, purity: 97.9%; 1H NMR (400 MHz, DMSO- d_6): δ 11.31 (s, 1H, *NH*-OH), 9.14 (s, 1H, OH), 7.69–7.28 (m, 4H, arom., NH), 7.12–6.87 (m, 3H, arom.), 4.67/4.51 (2 x s, 2H, CH₂), 3.88/3.69 (2 x s, 2H, CH₂), 2.27 (s, 6H, 2 x CH₃), 1.42/1.24/1.21 (s, 9H, *t*-Bu) ppm; ^{13}C NMR (101 MHz, DMSO- d_6): δ 171.6, 166.6, 162.6, 161.3, 161.1, 158.9, 137.6, 137.5, 136.0, 133.8, 131.5, 131.4, 130.8, 129.9, 128.8, 128.7, 127.4, 127.3, 124.1, 123.5, 123.0, 113.8, 113.6, 51.6, 50.2, 43.1, 28.5, 28.4, 20.8 ppm; HRMS (m/z): M^- calcd for C₂₃H₂₈FN₃O₄ 428.1991, found 428.1992.

4-({*N*-[(*tert*-Butylcarbamoyl)methyl]-1-[4-(dimethylamino)phenyl]formamido}methyl)-3-fluoro-*N*-hydroxybenzamide (10j).

Synthesis according to general procedure B using *tert*-butyl isocyanide (0.06 mL) afforded **10j** as an off-white solid (85.0 mg, 0.19 mmol, 38%); mp 132 °C; t_R : 6.10 min, purity: 95.5%; 1H NMR (400 MHz, DMSO- d_6 , 20 °C): δ 11.22 (s, 1H, *NH*-OH), 9.14 (s, 1H, OH), 7.71–7.23 (m, 6H, arom., NH), 6.78–6.62 (m, 2H, arom.), 4.63 (s, 2H, CH₂), 3.82 (s, 2H, CH₂), 2.93 (s, 6H, NMe₂), 1.22 (s, 9H, *t*-Bu) ppm; ^{13}C NMR (101 MHz, DMSO- d_6): δ 171.7, 169.3, 167.3, 162.5, 161.3, 151.3, 133.7, 131.5, 131.4, 129.7, 128.8, 128.7, 127.7,

127.5, 123.0, 122.0, 113.8, 113.6, 111.0, 58.4, 50.3, 49.9, 28.43, 28.38 ppm; HRMS (m/z): MNa^+ calcd for $C_{23}H_{29}FN_4O_4$ 467.2065, found 467.2071.

4-({N-[(*tert*-Butylcarbamoyl)methyl]-1-(2-fluorophenyl)formamido)methyl}-3-fluoro-*N*-hydroxybenzamide (10k).

Synthesis according to general procedure A using 2-fluorobenzoic acid (70.0 mg) and *tert*-butyl isocyanide (0.06 mL) afforded **10k** as an orange solid (133 mg, 0.32 mmol, 63%); mp 111 °C; t_R : 7.10 min, purity: 96.8%; 1H NMR (400 MHz, DMSO- d_6 , 20 °C): δ 9.21 (s, 1H, OH), 7.73–7.12 (m, 8H, arom. NH), 4.72/4.47 (s, 2H, CH_2), 3.95/3.75 (2 x s, 2H, CH_2), 1.44/1.24/1.17/1.14 (4 x s, 9H, *t*-Bu) ppm; ^{13}C NMR (101 MHz, DMSO- d_6): δ 166.9, 166.4, 166.1, 162.5, 161.3, 161.2, 158.9, 158.7, 134.4, 134.0, 133.9, 131.5, 131.4, 129.9, 129.6, 128.8, 128.7, 128.5, 127.1, 126.9, 126.1, 124.8, 124.6, 124.0, 123.9, 122.9, 115.9, 115.7, 113.8, 113.6, 51.2, 50.2, 47.3, 46.9, 43.3, 28.5, 28.3, 27.9 ppm; HRMS (m/z): M^- calcd for $C_{21}H_{23}F_2N_3O_4$ 418.1584, found 418.1584.

4-({N-[(*tert*-Butylcarbamoyl)methyl]-1-(2-methylphenyl)formamido)methyl}-3-fluoro-*N*-hydroxybenzamide (10l).

Synthesis according to general procedure A using 2-methylbenzoic acid (68.0 mg) and *tert*-butyl isocyanide (0.06 mL) afforded **10l** as an off-white solid (105 mg, 0.25 mmol, 50%); mp 109 °C; t_R : 7.24 min, purity: 96.4%; 1H NMR (300 MHz, DMSO- d_6 , 60 °C): δ 11.05 (s, 1H, *NH*-OH), 8.98 (s, 1H, OH), 7.70–7.12 (m, 8H, arom., NH), 4.74/4.41 (2 x s, 2H, CH_2), 3.93/3.60 (2x s, 2H, CH_2), 2.30/2.22 (2 x s, 3H, CH_3), 1.47/1.27/1.18/1.17 (s, 9H, *t*-Bu) ppm; ^{13}C NMR (101 MHz, DMSO- d_6): δ 171.2, 171.0, 166.5, 162.5, 162.3, 135.9, 134.3, 134.0, 133.94, 133.86, 132.0, 131.5, 131.4, 130.3, 129.8, 128.83, 128.78, 128.7, 127.4, 127.2, 125.7, 125.6, 125.5, 123.0, 113.9, 113.6, 51.0, 50.2, 46.7, 46.5, 42.7, 28.5, 28.3, 18.5 ppm; HRMS (m/z): M^- calcd for $C_{22}H_{26}FN_3O_4$ 414.1835, found 414.1835.

4-({N-[(*tert*-Butylcarbamoyl)methyl]-1-(2-methoxyphenyl)formamido)methyl}-3-fluoro-*N*-hydroxybenzamide (10m).

Synthesis according to general procedure A using 2-methoxybenzoic acid (76.0 mg) and *tert*-butyl isocyanide (0.06 mL) afforded **10m** as a white solid (83.0 mg, 0.19 mmol, 38%); mp 126 °C; t_R : 7.54 min, purity: 95.6%; 1H NMR (300 MHz, DMSO- d_6 , 60 °C): δ 9.46–8.85 (br s, 1H, OH), 7.71–6.80 (m, 8H, arom., NH), 4.42 (s, 1H, CH_2), 4.01–3.40 (m, 6H, OCH_3 , 2 x CH_2), 1.47–1.09 (m, 9H, *t*-Bu) ppm; ^{13}C NMR (101 MHz, DMSO- d_6): δ 169.4, 169.3, 169.1, 166.7, 166.5, 162.6, 161.2, 158.7, 154.9, 154.7, 154.5, 134.0, 133.6, 133.5, 132.1, 131.5, 131.4, 130.7, 130.6, 130.4, 129.1, 129.0, 128.8, 128.7, 127.8, 127.7, 127.5, 127.4, 125.4, 125.1, 123.0, 122.8, 122.7, 120.6, 120.5, 113.7, 113.4, 111.5, 111.4, 55.6, 55.3, 51.0, 50.2, 47.7, 46.5, 42.6, 42.6, 28.5, 28.3 ppm; HRMS (m/z): M^- calcd for $C_{22}H_{26}FN_3O_5$ 430.1784, found 430.1784.

4-({N-[(*tert*-Butylcarbamoyl)methyl]-1-[2-(trifluoromethyl)phenyl]formamido)methyl}-3-fluoro-*N*-hydroxybenzamide (10n).

Synthesis according to general procedure A using 2-(trifluoromethyl)benzoic acid (95.0 mg) and *tert*-butyl isocyanide (0.06 mL) afforded **10n** as a yellow solid (103 mg, 0.22 mmol,

44%); mp 137 °C; t_R : 7.03 min, purity: 95.1%; 1H NMR (300 MHz, DMSO- d_6 , 60 °C): δ 10.91 (s, 1H, *NH*-OH), 9.00 (s, 1H, OH), 7.89–7.17 (m, 8H, arom., NH), 5.11/4.47 (2 x s, 2H, CH₂), 3.90/3.57 (2 x s, 2H, CH₂), 1.46/1.26/1.18 (3 x s, 9H, *t*-Bu) ppm; ^{13}C NMR (75 MHz, DMSO- d_6): δ 168.5, 166.4, 166.2, 162.5, 162.4, 161.8, 134.4, 134.32, 134.29, 134.1, 134.04, 133.99, 132.71, 132.68, 132.6, 132.06, 132.05, 132.0, 131.5, 131.4, 130.52, 130.45, 130.4, 129.8, 129.7, 128.8, 128.7, 127.73, 127.67, 127.6, 126.8, 126.6, 126.51, 126.49, 126.4, 125.2, 124.8, 122.9, 122.81, 122.79, 121.8, 113.91, 113.87, 113.6, 50.8, 50.3, 42.7, 42.6, 28.5, 28.3 ppm; HRMS (m/z): M^- calcd for C₂₂H₂₃F₄N₃O₄ 468.1552, found 468.1548.

4-({*N*-[(*tert*-Butylcarbamoyl)methyl]-1-(2-chlorophenyl)formamido)methyl}-3-fluoro-*N*-hydroxybenzamide (10o).

Synthesis according to general procedure A using 2-chlorobenzoic acid (78.0 mg) and *tert*-butyl isocyanide (0.06 mL) afforded **10o** as a white solid (150 mg, 0.34 mmol, 69%); mp 145 °C; t_R : 7.27 min, purity: 98.6%; 1H NMR (400 MHz, DMSO- d_6 , 20 °C): δ 11.27 (s, 1H, *NH*-OH), 9.15 (s, 1H, OH), 7.71–7.24 (m, 8H, arom., NH), 5.27–5.05/4.73–4.22 (2 x m, 2H, CH₂), 4.05–3.79/3.72–3.52 (2 x m, 2H, CH₂), 1.24/1.14 (2 x s, 9H, *t*-Bu) ppm; ^{13}C NMR (101 MHz, DMSO- d_6): δ 168.3, 168.0, 166.3, 166.1, 162.5, 161.3, 161.2, 158.8, 158.7, 135.30, 135.27, 134.3, 134.2, 133.9, 133.9, 131.5, 131.4, 130.7, 130.6, 130.1, 130.04, 129.97, 129.9, 129.6, 129.4, 129.4, 128.9, 128.8, 128.7, 128.3, 128.1, 127.4, 127.3, 127.0, 126.9, 50.8, 50.3, 47.3, 46.6, 42.9, 42.9, 28.5, 28.3 ppm; HRMS (m/z): M^- calcd for C₂₁H₂₃ClFN₃O₄ 434.1288, found 434.1273.

4-({*N*-[(*tert*-Butylcarbamoyl)methyl]-1-[2-(propan-2-yl)phenyl]formamido)methyl}-3-fluoro-*N*-hydroxybenzamide (10p).

Synthesis according to general procedure A using 2-isopropylbenzoic acid (82.0 mg) and *tert*-butyl isocyanide (0.06 mL) afforded **10p** as a white solid (132 mg, 0.30 mmol, 60%); mp 130 °C; t_R : 7.96 min, purity: 96.4%; 1H NMR (400 MHz, DMSO- d_6 , 20 °C): δ 11.31 (s, 1H, *NH*-OH), 9.116 (s, 1H, OH), 7.68–7.09 (m, 8H, arom., NH), 4.98–4.82/4.64–4.08 (2 x m, 2H, CH₂), 3.81–3.70/3.66–3.48 (2 x m, 2H, CH₂), 3.12 (2 x p, $J = 6.7/6.9$ Hz, 1H, *i*-Pr-CH), 1.38–1.04 (m, 15H, *i*-Pr, *t*-Bu) ppm; ^{13}C NMR (101 MHz, DMSO- d_6): δ 171.1, 166.6, 166.5, 162.5, 161.4, 161.0, 159.0, 158.6, 145.1, 144.9, 135.0, 134.9, 134.0, 133.9, 131.5, 131.4, 129.6, 129.3, 129.2, 128.8, 128.7, 127.3, 127.2, 125.8, 125.7, 125.6, 125.5, 123.1, 123.0, 113.9, 113.7, 51.0, 50.3, 46.9, 42.3, 29.9, 29.8, 28.5, 28.3, 24.9, 24.2, 23.2, 22.8 ppm; HRMS (m/z): MNa^+ calcd for C₂₄H₃₀FN₃O₄ 466.2113, found 466.2128.

Crystallization.

Catalytic domain 2 of HDAC6 from *Danio rerio* (hereafter noted as simply “HDAC6”) was recombinantly expressed in *E. coli* BL21 (DE3) cells via inoculation with His-MBP-TEV-HDAC6-pET28a(+) vector. The protein was purified using techniques previously described.⁶⁴

The HDAC6-**10h** complex was crystallized via sitting drop vapor diffusion at 4 °C. Briefly, a 100-nL drop of protein solution [10 mg/mL HDAC6, 50 mM 4-(2-hydroxyethyl)-1-piperazineethanesulfonic acid (HEPES) (pH 7.5), 100 mM KCl, 5% glycerol (v/v), 1mM

tris(2-carboxyethyl)phosphine (TCEP), **10h** (2 mM), and 5% DMSO (v/v)] was added to a 100-nL drop of precipitant solution from the PEG/ION™ screen [2% v/v Tacsimate pH 8.0, 0.1 M Tris pH 8.5, and 16% w/v PEG 3,350] and equilibrated against 80 μ L of precipitant solution. Crystals appeared after 2 weeks and were soaked in a cryoprotectant solution comprised of the mother liquor solution and 20% ethylene glycol prior to looping and flash cooling in liquid nitrogen.

Data Collection and Structure Determination.

X-ray diffraction data for the HDAC6-**10h** complex were collected on the NSLS-II AMX beamline at Brookhaven National Laboratory. Data were indexed and integrated using iMosflm⁶⁵; calculation of the Patterson map and self-rotation function indicated the presence of pseudotranslation with a peak height ~28% of that of the origin peak. Weak reflections resulting from the pseudotranslation were removed during phasing and refinement. The structure was phased by molecular replacement using the atomic coordinates of unliganded HDAC6 (PDB 5EEM)¹⁹ as a search probe in the program Phaser.⁶⁶ The atomic structures were then modeled and refined using Coot⁶⁷ and Phenix⁶⁸ and the **10h** inhibitor was built into well-defined electron density in the final stages of refinement. The quality of the final model was evaluated with MolProbity.⁶⁹ Data collection and refinement statistics are recorded in Table S2 Atomic coordinates and crystallographic structure factors have been deposited in the Protein Data Bank with accession code 7U8Z.

Biological experiments

Cell Culture.

Leukemia cell lines HL60, MOLM13, MV4-11 (acute myeloid leukemia or AML), HAL01, REH, 697 (B-cell acute lymphoblastic leukemia or B-ALL), K562 (chronic myeloid leukemia), Jurkat (T-cell acute lymphoblastic leukemia) (DSMZ, Braunschweig, Germany) and two healthy fibroblast control cells (ATCC, Virginia, US) were cultured in RPMI 1640 GlutaMax medium supplemented with 10-20% FCS. All cell lines were grown at 37°C under humidified air supplemented with 5% CO₂.

Cell Viability Assay.

The CellTiter-Glo luminescent cell viability assay (Promega, Madison) was done to determine the IC₅₀ values of the tested compounds for every cell line. The different compounds were printed on white 384-well plates (Thermo Fisher Scientific, Waltham) with at least 5 different, increasing concentrations (5 nM – 25 μ M) using a digital dispenser (D300e, Tecan, Männedorf, Switzerland). The cell viability was monitored after 72 h using the CellTiter-Glo luminescent assay using a microplate reader (Spark, Tecan). The IC₅₀ values for the tested compounds were determined by plotting raw data (normalized to controls) using a sigmoid dose curve and nonlinear regression (GraphPad Prism Inc., San Diego, CA).

Combinatorial drug screening.

10h and decitabine were printed on white 384-well plates (Thermo Fisher Scientific, Waltham, USA) with increasing concentrations in a dose-response 8 x 8 matrices

using a digital dispenser (D300e, Tecan, Maennedorf, Switzerland). **10h** was printed in concentration range from 0.1 μM up to 2 μM and for decitabine from 0.25 μM up to 10 μM , in a logarithmic distribution. The viability was monitored after 72 h using CellTiter-Glo luminescent assay (as described above), using a microplate reader (Spark, Tecan). The ZIP synergy scores calculations were based on the ZIP model⁷⁰ using the Synergy Finder tool (<https://synergyfinder.fimm.fi/>).

Annexin-V staining.

For evaluating apoptosis, cells treated with respective compounds or control at the indicated concentrations for 48 h were stained with annexin V and PI and later subjected to FACS analysis, following supplier's guidelines (Invitrogen, Carlsbad, CA).

Immunoblotting.

Whole-cell lysates were produced after 24 h treatment with the respective compounds under standard culture conditions. Afterwards, whole-cell lysates were immunoblotted using anti-acetyl- α -tubulin (no. 5335), anti-acetyl-histone H3 (no. 9677S), and anti- β -Actin (no. 5125S) or anti-GAPDH (no. 97166), following supplier's guidelines (Cell Signaling Technology, Danvers, MA).

Inhibition assay for HDAC1-3 and HDAC6.

In vitro inhibitory activities against human HDAC1, HDAC2, HDAC3/NcoR2, and HDAC6 were measured using a previously published protocol.⁷¹ In short, OptiPlate-96 black microplates (Perkin Elmer) were used with an assay volume of 50 μL . 5 μL test compound or control, diluted in assay buffer (50 mM Tris-HCl, pH 8.0, 137 mM NaCl, 2.7 mM KCl, 1 mM MgCl_2 , 0.1 mg/mL BSA), were incubated with 35 μL of the fluorogenic substrate ZMAL (Z-Lys(Ac)-AMC)⁷² (21.43 μM in assay buffer) and 10 μL of human recombinant HDAC1 (BPS Bioscience, Catalog# 50051), HDAC2 (BPS Bioscience, Catalog# 50052), HDAC3/NcoR2 (BPS Bioscience, Catalog# 50003) or full length HDAC6 (BPS Bioscience, Catalog# 50006) at 37 °C. After an incubation time of 90 min, 50 μL of 0.4 mg/mL trypsin in trypsin buffer (50 mM Tris-HCl, pH 8.0, 100 mM NaCl) were added, followed by further incubation at 37 °C for 30 min. Fluorescence was measured with an excitation wavelength of 355 nm and an emission wavelength of 460 nm using a Fluoroskan Ascent microplate reader (Thermo Scientific). All compounds were evaluated in duplicates in at least two independent experiments

HDAC4 inhibition assay.

In vitro inhibitory activities against HDAC4 were determined using a HDAC4 assay protocol adapted from Asfaha *et al.*⁷³ For compounds and controls, 3-fold serial dilutions of the respective DMSO-stock solutions were prepared in assay buffer (50 mM Tris-HCl, pH 8.0, 137 mM NaCl, 2.7 mM KCl, 1.0 mM $\text{MgCl}_2 \cdot 6 \text{H}_2\text{O}$, 0.1 mg/mL BSA). 5.0 μL of these serial dilutions were transferred into 96-well microplates (OptiPlate-96 Black, PerkinElmer). 35 μL of the fluorogenic substrate Boc-Lys(Tfa)-AMC (Bachem, Catalog# 4060676, 42.86 μM in assay buffer) and 10 μL of HDAC4 (BPS Bioscience, Catalog# 50004) enzyme solution were added. The total assay volume (50 μL , max. 1% DMSO) was incubated at

37 °C for 90 min. Subsequently, 50 µL of trypsin (1.0 mg/mL) in trypsin buffer (50 mM Tris-HCl, pH 8.0, 100 mM NaCl) were added, followed by additional 30 min of incubation at 37 °C. Fluorescence (excitation: 355 nm, emission: 460 nm) was measured using a FLUOstar OPTIMA microplate reader (BMG LABTECH). IC₅₀ values were determined by generating normalized dose-response curves using the build-in “*log(inhibitor) vs. response (three parameters)*” equation provided by GraphPad Prism (GraphPad Prism 9.0, San Diego, USA). All compounds were tested in duplicates, reported mean IC₅₀ values, including standard deviation, are calculated from at least two independent experiments. TMP269⁷⁴ (Selleck Chemicals, Catalog# S7324) was used as control compound (IC₅₀ = 0.488 ± 0.049 µM).

PAINS Analysis.

We filtered all compounds for pan-assay interference compounds (PAINS) using the online filter <http://zinc15.docking.org/patterns/home/>.⁷⁵ No compound was flagged as PAINS.

Supplementary Material

Refer to Web version on PubMed Central for supplementary material.

ACKNOWLEDGMENTS

This work is based on research conducted at beamline 17-ID-1 (AMX) of the National Synchrotron Light Source II, a Department of Energy (DOE) Office of Science User Facility operated for the DOE Office of Science by Brookhaven National Laboratory under Contract DE-SC0012704. The Center for BioMolecular Structure (CBMS) is primarily supported by the National Institutes of Health, National Institute of General Medical Sciences (NIGMS), through a Center Core P30 Grant (P30GM133893) and by the DOE Office of Biological and Environmental Research (KP1607011).

Funding Sources

This work was supported by the Deutsche Forschungsgemeinschaft (DFG) (HA 7783/1-1 and 7783/1-2 to FKH) and the US National Institutes of Health (grant GM49758 to D.W.C.). S.B. acknowledges the financial support by Forschungskommission (2021-19) and DSO-Netzwerkverbundes, HHU Düsseldorf. This study was funded in part by KinderKrebsForschung e.V and the Deutsche Forschungsgemeinschaft (DFG, German Research Foundation) – 270650915 (Research Training Group GRK 2158, TP2d to SB). A.B. is supported by the TransOnc priority program of the German Cancer Aid within grant #70112951 (ENABLE). AB additionally acknowledges the financial support from Löwenstern e.V. and from Katharina-Hardt Foundation.

ABBREVIATIONS

AIBN	azobisisobutyronitrile
CDCl₃	chloroform- <i>d</i>
DMF	dimethylformamide
DMSO	dimethylsulfoxide
DCM	dichloromethane
Et₂O	diethyl ether
EtOAc	ethyl acetate

MeOH	methanol
min	minutes
NBS	<i>N</i> -bromosuccinimide
petrol	petroleum ether
rt	room temperature
TFA	trifluoroacetic acid
THF	tetrahydrofuran
U4CR	Ugi 4-component reaction

REFERENCES

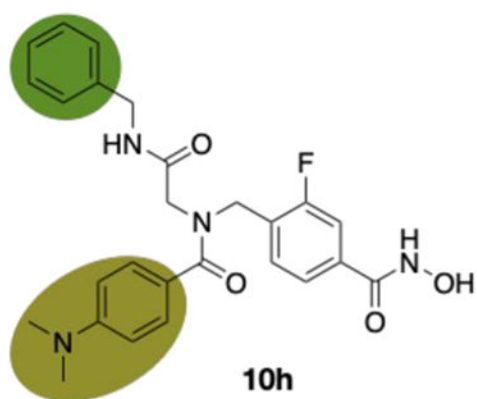
- 1). Biel M; Wascholowski V; Giannis A Epigenetics – an epicenter of gene regulation: Histones and histone-modifying enzymes. *Angew. Chem. Int. Ed* 2005, 44, 3186–3216.
- 2). Bannister AJ; Kouzarides T Regulation of chromatin by histone modifications. *Cell. Res* 2011, 21, 381–395. [PubMed: 21321607]
- 3). Bertrand P Inside HDAC with HDAC inhibitors. *Eur. J. Med. Chem* 2010, 45, 2095–2116. [PubMed: 20223566]
- 4). Xiao H; Jiao J; Wang L; O'Brien S; Newick K; Wang L-CS, Falkensammer E; Liu Y; Han R; Kapoor V; Hansen FK; Kurz T; Hancock WW; Beier UH HDAC5 controls the functions of Foxp3+ T-regulatory and CD8+ T cells. *Int. J. Cancer* 2016, 138, 2477–2486. [PubMed: 26704363]
- 5). Huang J; Wang L; Dahiya S; Beier UH; Han R; Samanta A; Bergman J; Sotomayor EM; Seto E; Kozikowski AP; Hancock WW Histone/protein deacetylase 11 targeting promotes Foxp3+ Treg function. *Sci. Rep* 2017, 7, 8626. [PubMed: 28819166]
- 6). Wang P; Wang Z; Liu J Role of HDACs in normal and malignant hematopoiesis. *Mol. Cancer* 2020, 19, 5. [PubMed: 31910827]
- 7). Mielcarek M; Zielonka D; Carnemolla A; Marcinkowski JT; Guidez F HDAC4 as a potential therapeutic target in neurodegenerative diseases: a summary of recent achievements. *Front. Cell. Neurosci* 2015, 9, 42. [PubMed: 25759639]
- 8). Roche J; Bertrand P Inside HDACs with more selective HDAC inhibitors. *Eur. J. Med. Chem* 2016, 121, 451e483. [PubMed: 27318122]
- 9). Witt O; Deubzer HE; Milde T; Oehme I HDAC family: What are the cancer relevant targets? *Canc. Lett* 2009, 277, 8–21.
- 10). Jenke R; Reßing N; Hansen FK; Aigner A; Büch T Anticancer Therapy with HDAC Inhibitors: Mechanism-Based Combination Strategies and Future Perspectives. *Cancers* 2021, 23, 634.
- 11). Stoszko M; Ne E; Abner E; Mahmoudi T A broad drug arsenal to attack a strenuous latent HIV reservoir. *Curr. Opin. Virol* 2019, 38, 37–53. [PubMed: 31323521]
- 12). Aldana-Masangkay GI; Sakamoto KM The role of HDAC6 in cancer. *J. Biomed. Biotechnol* 2011, 2011, 875824. [PubMed: 21076528]
- 13). Li T; Zhang C; Hassan S; Liu X; Song F; Chen K; Zhang W; Yang J Histone deacetylase 6 in cancer. *J. Hematol. Oncol* 2018, 11, 111. [PubMed: 30176876]
- 14). Kalin JH; Bergman JA Development and therapeutic implications of selective histone deacetylase 6 inhibitors. *J. Med. Chem* 2013, 56, 6297–6313. [PubMed: 23627282]
- 15). Simões-Pires C; Zwick V; Nurisso A; Schenker E; Carrupt P-A; Cuendet M HDAC6 as a target for neurodegenerative diseases: what makes it different from the other HDACs?. *Mol. Neurodegener* 2013, 8, 7. [PubMed: 23356410]

- 16). Sellmer A; Stangl H; Beyer M; Grünstein E; Leonhardt M; Pongratz H; Eichhorn E; Elz S; Striegl B; Jenei-Lanzl Z; Dove S; Straub RH; Krämer OH; Mahboobi S Marbostat-100 defines a new class of potent and selective antiinflammatory and antirheumatic histone deacetylase 6 inhibitors. *J. Med. Chem* 2018, 61, 3454–3477. [PubMed: 29589441]
- 17). Shen S; Kozikowski AP A patent review of histone deacetylase 6 inhibitors in neurodegenerative diseases (2014-2019). *Expert Opin. Ther. Pat* 2020, 30, 121–136. [PubMed: 31865813]
- 18). Zhang X-H; Qin-Ma; Wu HP; Khamis MY; Li Y-H; Ma L-Y; Liu H-M A Review of progress in histone deacetylase 6 inhibitors research: Structural specificity and functional diversity. *J. Med. Chem* 2021, 64, 1362–1391. [PubMed: 33523672]
- 19). Hai Y; Christianson DW; Histone deacetylase 6 structure and molecular basis of catalysis and inhibition. *Nat. Chem. Biol* 2016, 12, 741–747. [PubMed: 27454933]
- 20). Zou H; Wu Y; Navre M; Sang B-C Characterization of the two catalytic domains in histone deacetylase 6. *Biochem. Biophys. Res. Commun* 2006, 341, 45–50. [PubMed: 16412385]
- 21). Osko JD; Christianson DW Structural basis of catalysis and inhibition of HDAC6 CD1, the enigmatic catalytic domain of histone deacetylase 6. *Biochemistry* 2019, 58, 4912–4924. [PubMed: 31755702]
- 22). Hubbert C; Guardiola A; Shao R; Kawaguchi Y; Ito A; Nixon A; Yoshida M; Wang X-F; Yao TP HDAC6 is a microtubule-associated deacetylase. *Nature* 2002, 417, 455–458. [PubMed: 12024216]
- 23). Zhang X; Yuan Z; Zhang Y; Yong S; Salas-Burgos A; Koomen J; Olashaw N; Parsons JT; Yang X-J; Dent SR; Yao T-P; Lane WS; Seto E HDAC6 modulates cell motility by altering the acetylation level of cortactin. *Mol. Cell* 2007, 27, 197–213. [PubMed: 17643370]
- 24). Valenzuela-Fernández A; Cabrero JR; Serrador JM; Sánchez-Madrid F HDAC6: a key regulator of cytoskeleton, cell migration and cell-cell interactions. *Trends Cell Biol* 2008, 18, 291–297. [PubMed: 18472263]
- 25). Zhang Y; Li N; Caron C; Matthias G; Hess D; Khochbin S; Matthias P HDAC-6 interacts with and deacetylates tubulin and microtubules in vivo. *EMBO J* 2003, 22, 1168–1179. [PubMed: 12606581]
- 26). Bali P; Pranpat M; Bradner J; Balasis M; Fiskus W; Guo F; Rocha K; Kumaraswamy S; Boyapalle S; Atadja P; Seto E; Bhalla K Inhibition of histone deacetylase 6 acetylates and disrupts the chaperone function of heat shock protein 90. *J. Biol. Chem* 2005, 280, 26729–26734. [PubMed: 15937340]
- 27). Kawaguchi Y; Kovacs JJ; McLaurin A; Vance JM; Ito A; Yao T-P The deacetylase HDAC6 regulates aggresome formation and cell viability in response to misfolded protein stress. *Cell* 2003, 115, 727–738. [PubMed: 14675537]
- 28). Huber EM; Groll M Inhibitors for the immuno- and constitutive proteasome: Current and future trends in drug development. *Angew. Chem. Int. Ed* 2012, 51, 8708–8720.
- 29). Depetter Y; Geurs S; De Vreese R; Goethals S; Vandoorn E; Laevens A; Steenbrugge J; Meyer E; de Tullio P; Bracke M; D’hooghe M; De Wever O Selective pharmacological inhibitors of HDAC6 reveal biochemical activity but functional tolerance in cancer models. *Int. J. Cancer* 2019, 145, 735–774. [PubMed: 30694564]
- 30). Suraweera A; O’Byrne KJ; Richard DJ Combination therapy with histone deacetylase inhibitors (HDACi) for the treatment of cancer: Achieving the full therapeutic potential of HDACi. *Front. Oncol* 2018, 8, 92. [PubMed: 29651407]
- 31). Kumagai T; Wakimoto N; Yin D; Gery S; Kawamata N; Takai N; Komatsu N; Chumakov A; Imai Y; Koeffler HP Histone deacetylase inhibitor, suberoylanilide hydroxamic acid (Vorinostat, SAHA) profoundly inhibits the growth of human pancreatic cancer cells. *Int. J. Cancer* 2007, 121, 656–665, [PubMed: 17417771]
- 32). Leshchenko VV; Kuo P-Y; Shaknovich R; Yang DT; Gellen T; Petrich A; Yu Y; Remache Y; Weniger MA; Rafiq S; Suh KS; Goy A; Wilson W; Verma A; Braunschweig I; Muthusamy N; Kahl BS; Byrd JC; Wiestner A; Melnick A; Parekh S Genomewide DNA methylation analysis reveals novel targets for drug development in mantle cell lymphoma. *Blood* 2010, 116, 1025–1034. [PubMed: 20427703]

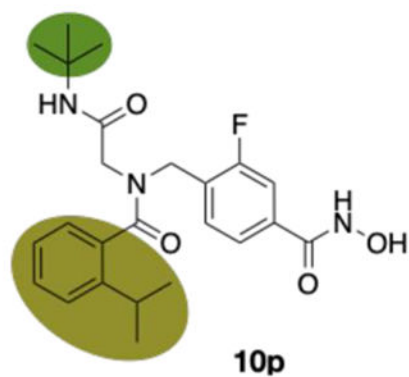
- 33). Kalac M; Scotto L; Marchi E; Amengual J; Seshan VE; Bhagat G; Ulahannan N; Leshchenko VV; Temkin AM; Parekh S; Tycko B; O'Connor OA HDAC inhibitors and decitabine are highly synergistic and associated with unique gene-expression and epigenetic profiles in models of DLBCL. *Blood* 2011, 118, 5506–5516. [PubMed: 21772049]
- 34). NCT04514081.
- 35). NCT04233294.
- 36). NCT04337606.
- 37). Purser S; Moore PR; Swallow S; Gouverneur V Fluorine in medicinal chemistry. *Chem. Soc. Rev* 2008, 37, 320–330. [PubMed: 18197348]
- 38). Mei H; Han J; Fustero S; Medio-Simon M; Sedgwick DM; Santi C; Ruzziconi R; Soloshonok VA Fluorine-containing drugs approved by the FDA in 2018. *Chem. Eur. J* 2019, 25, 11797–11819. [PubMed: 31099931]
- 39). Müller K; Faeh C; Diederich F Fluorine in pharmaceuticals: Looking beyond intuition. *Science* 2007, 317, 1881–1886. [PubMed: 17901324]
- 40). Meanwell NA Fluorine and fluorinated motifs in the design and application of bioisosteres for drug design. *J. Med. Chem* 2018, 61, 5822–5880. [PubMed: 29400967]
- 41). Johnson BM; Shu Y-Z; Zhuo X; Meanwell NA Metabolic and pharmaceutical aspects of fluorinated compounds. *J. Med. Chem* 2020, 63, 6315–6386. [PubMed: 32182061]
- 42). Pan Y The dark side of fluorine. *ACS Med. Chem. Lett* 2019, 10, 1016–1019. [PubMed: 31312400]
- 43). Diedrich D; Hamacher A; Gertzen CGW; Alves Avelar LA; Reiss GJ; Kurz T; Gohlke H; Kassack MU; Hansen FK Rational design and diversity-oriented synthesis of peptoid-based selective HDAC6 inhibitors. *Chem. Commun* 2016, 52, 3219–3222.
- 44). Strebl MG, Campbell AJ, Zhao W-N, Schroeder FA, Riley MA, Chindavong PS, Morin TM, Haggarty SJ, Wagner FF, Ritter T, Hooker JM HDAC6 brain mapping with [18F]Bavastat enabled by a Ru-mediated deoxyfluorination. *ACS Cent. Sci* 2017, 3, 1006–1014. [PubMed: 28979942]
- 45). Porter NJ; Osko JD; Diedrich D; Kurz T; Hooker JM; Hansen FK; Christianson DW Histone deacetylase 6-selective inhibitors and the influence of capping groups on hydroxamate-zinc denticity. *J. Med. Chem* 2018, 61, 8054–8060. [PubMed: 30118224]
- 46). Wang C; Schroeder FA; Wey H-Y; Borra R; Wagner FF; Reis S; Kim SW; Holson EB; Haggarty SJ; Hooker JM In vivo imaging of histone deacetylases (HDACs) in the central nervous system and major peripheral organs. *J. Med. Chem* 2014, 57, 7999–8009. [PubMed: 25203558]
- 47). Sandrone G; Cukier CD; Zrubek K; Marchini M; Vergani B; Caprini G; Fossati G; Steinkühler C; Stevenazzi A Role of Fluorination in the Histone Deacetylase 6 (HDAC6) Selectivity of Benzohydroxamate-Based Inhibitors. *ACS Med. Chem. Lett* 2021, 12, 1810–1817. [PubMed: 34795871]
- 48). Mackwitz MKW; Hesping E; Antonova-Koch Y; Diedrich D; Gebru T; Skinner-Adams T; Clarke M; Schöler A; Limbach L; Kurz T; Winzeler EA; Held J; Andrews KT; Hansen FK Structure-activity and structure-toxicity relationships of novel peptoid based histone deacetylase inhibitors with dual-stage antiplasmodial activity. *ChemMedChem* 2019, 14, 912–926. [PubMed: 30664827]
- 49). Reßing N; Sönnichsen M; Osko JD; Schöler A; Schliehe-Diecks J; Skerhut A; Borkhardt A; Hauer J; Kassack MU; Christianson DW; Bhatia S; Hansen FK Multicomponent Synthesis, Binding Mode, and Structure–Activity Relationship of Selective Histone Deacetylase 6 (HDAC6) Inhibitors with Bifurcated Capping Groups. *J. Med. Chem* 2020, 63, 10339–10351. [PubMed: 32803970]
- 50). Schmidt J; Rotter M; Weiser T; Wittmann S; Weizel L; Kaiser A; Heering J; Goebel T; Angioni C; Wurglics M; Paulke A; Geisslinger G; Kahnt A; Steinhilber D; Proschak E; Merk D A dual modulator of Farnesoid X receptor and soluble epoxide hydrolase to counter nonalcoholic steatohepatitis. *J. Med. Chem* 2017, 60, 7703–7724. [PubMed: 28845983]
- 51). Diedrich D; Stenzel K; Hesping E; Antonova-Koch Y; Gebru T; Duffy S; Fisher G; Schöler A; Meister S; Kurz T; Avery VM; Winzeler E; Held J; Andrews KT; Hansen FK One-pot, multi-component synthesis and structure-activity relationships of peptoid-based histone deacetylase

- (HDAC) inhibitors targeting malaria parasites. *Eur. J. Med. Chem* 2018, 158, 801–813. [PubMed: 30245402]
- 52). Reßing N; Marquardt V; Gertzen CGW; Schöler A; Schramm A; Kurz T; Gohlke H; Aigner A; Remke M; Hansen FK Design, synthesis and biological evaluation of β -peptoid-capped HDAC inhibitors with anti-neuroblastoma and anti-glioblastoma activity. *Med. Chem. Commun* 2019, 10, 1109–1115.
- 53). Mackwitz MKW; Hamacher A; Osko JD; Held J; Schöler A; Christianson DW; Kassack MU; Hansen FK Multicomponent synthesis and binding mode of imidazo[1,2-pubs.acs.org/jmc Article a]pyridine-capped selective HDAC6 inhibitors. *Org. Lett* 2018, 20, 3255–3258. [PubMed: 29790770]
- 54). Gaisina IN; Tueckmantel W; Ugolkov A; Shen S; Hoffen J; Dubrovskiy O; Mazar A; Schoon RA; Billadeau D; Kozikowski AP Identification of HDAC6-selective inhibitors of low cancer cell cytotoxicity. *ChemMedChem* 2016, 11, 81–92. [PubMed: 26592932]
- 55). Robey RW; Chakraborty AR; Basseville A; Luchenko V; Bahr J; Zhan Z; Bates SE Histone deacetylase inhibitors: emerging mechanisms of resistance. *Mol. Pharmaceutics* 2011, 8, 2021–2031.
- 56). Lee J-H; Choy ML; Marks PA Chapter Two - mechanisms of resistance to histone deacetylase inhibitors. *Adv. Cancer Res* 2012, 116, 39–86. [PubMed: 23088868]
- 57). Alves Avelar LA; Schrenk C; Sönnichsen M; Hamacher A; Hansen FK; Schliehe-Diecks J; Borkhardt A; Bhatia S; Kassack MU; Kurz T Synergistic induction of apoptosis in resistant head and neck carcinoma and leukemia by alkoxyamide-based histone deacetylase inhibitors. *Eur. J. Med. Chem* 2021, 211, 113095. [PubMed: 33360560]
- 58). Bhatia S; Krieger V; Groll M; Osko JD; Reßing N; Ahlert H; Borkhardt A; Kurz T; Christianson DW; Hauer J; Hansen FK Discovery of the first-in-class dual histone deacetylase- proteasome inhibitor. *J. Med. Chem* 2018, 61, 10299–10309. [PubMed: 30365892]
- 59). Selg C; Schöler A; Schliehe-Diecks J; Hanl M; Sinatra L; Borkhardt A; Sárosi MB; Bhatia S; Hey-Hawkins E; Hansen FK Borinostats: solid-phase synthesis of carborane-capped histone deacetylase inhibitors with a tailor-made selectivity profile. *Chem. Sci* 2021, 12, 11873–11881. [PubMed: 34659728]
- 60). Yang H; Hoshino K; Sanchez-Gonzalez B; Kantarjian H; Garcia-Manero G Antileukemia activity of the combination of 5-aza-2'-deoxycytidine with valproic acid. *Leuk. Res* 2005, 29, 739–748. [PubMed: 15927669]
- 61). Kuendgen A; Lübbert M Current status of epigenetic treatment in myelodysplastic syndromes. *Ann. Hematol* 2008, 87, 601–611. [PubMed: 18392623]
- 62). Ianevski A; He L; Aittokallio T; Tang J SynergyFinder: a web application for analyzing drug combination dose-response matrix data. *Bioinformatics* 2017, 33, 2413–2415. [PubMed: 28379339]
- 63). Jiang X; Lee GT; Prasad K; Repi O A practical synthesis of a diazepinylbenzoic acid, a retinoid X receptor antagonist. *Org. Process Res. Dev* 2008, 12, 1137–1141.
- 64). Osko JD; Christianson DW Methods for the expression, purification, and crystallization of histone deacetylase 6–inhibitor complexes. *Methods Enzymol.* 2019, 626, 447–474. [PubMed: 31606087]
- 65). Battye TGG; Kontogiannis L; Johnson O; Powell HR; Leslie AGW iMOSFLM: a new graphical interface for diffraction-image processing with MOSFLM. *Acta Crystallogr. D. Biol. Crystallogr* 2011, 67, 271–281. [PubMed: 21460445]
- 66). McCoy AJ; Grosse-Kunstleve RW; Adams PD; Winn MD; Storoni LC; Read RJ Phaser crystallographic software. *J. Appl. Crystallogr* 2007, 40, 658–674. [PubMed: 19461840]
- 67). Emsley P; Lohkamp B; Scott WG; Cowtan K Features and development of Coot. *Acta Crystallogr. D. Biol. Crystallogr* 2010, 66, 486–501. [PubMed: 20383002]
- 68). Adams PD; Afonine PV; Bunkóczi G; Chen VB; Davis IW; Echols N; Headd JJ; Hung LW; Kapral GJ; Grosse-Kunstleve RW; McCoy AJ; Moriarty NW; Oeffner R; Read RJ; Richardson DC; Richardson JS; Terwilliger TC; Zwart PH PHENIX: a comprehensive Python-based system for macromolecular structure solution. *Acta Crystallogr. D Biol. Crystallogr* 2010, 66, 213–21. [PubMed: 20124702]

- 69). Chen VB; Arendall WB; Headd JJ; Keedy DA; Immormino RM; Kapral GJ; Murray LW; Richardson JS; Richardson DC MolProbity: all-atom structure validation for macromolecular crystallography. *Acta Crystallogr. D. Biol. Crystallogr* 2010, 66, 12–21. [PubMed: 20057044]
- 70). Ianebski A; He L; Aittokallio T; Tang J SynergyFinder: a web application for analyzing drug combination dose-response matrix data. *Bioinformatics* 2020, 36, 2645. [PubMed: 32118251]
- 71). Erdeljac N; Bussmann K; Schöler A; Hansen FK; Gilmour R Fluorinated Analogues of the Histone Deacetylase Inhibitor Vorinostat (Zolinza): Validation of a Chiral Hybrid Bioisostere, BITE. *ACS Med. Chem. Lett* 2019, 10, 1336–1340. [PubMed: 31531206]
- 72). Heltweg B; Dequiedt F; Verdin E; Jung M Nonisotopic substrate for assaying both human zinc and NAD⁺-dependent histone deacetylases. *Anal. Biochem* 2003, 319, 42–48. [PubMed: 12842105]
- 73). Asfaha Y; Schrenk C; Alves Avelar LA; Lange F; Wang C; Bandolik JJ; Hamacher A; Kassack MU; Kurz T Novel alkoxyamide-based histone deacetylase inhibitors reverse cisplatin resistance in chemoresistant cancer cells. *Bioorg. Med. Chem* 2020, 28, 115108. [PubMed: 31787463]
- 74). Lobera M; Madauss KP; Pohlhaus DT; Wright QG; Trocha M; Schmidt DR; Baloglu E; Trump RP; Head MS; Hofmann GA; Murray-Thompson M; Schwartz B; Chakravorty S; Wu Z; Mander PK; Kruidenier L; Reid RA; Burkhardt W; Turunen BJ; Rong JX; Wagner C; Moyer MB; Wells C; Hong X; Moore JT; Williams JD; Soler D; Ghosh S; Nolan MA Selective class IIa histone deacetylase inhibition via a nonchelating zinc-binding group. *Nat. Chem. Biol* 2013, 9, 319–325. [PubMed: 23524983]
- 75). Baell JB; Holloway GA New substructure filters for removal of pan assay interference compounds (PAINS) from screening libraries and for their exclusion in bioassays. *J. Med. Chem* 2010, 53, 2719–2740. [PubMed: 20131845]



HDAC1 IC₅₀: 0.013 ± 0.001 μM (SI^{1/6}: 1.3)
 HDAC2 IC₅₀: 0.014 ± 0.0001 μM (SI^{2/6}: 1.4)
 HDAC3 IC₅₀: 0.021 ± 0.002 μM (SI^{3/6}: 2.1)
 HDAC4 IC₅₀: 1.88 ± 0.12 μM (SI^{4/6}: 188)
 HDAC6 IC₅₀: 0.010 ± 0.00004 μM



HDAC1 IC₅₀: 8.01 ± 0.22 μM (SI^{1/6}: 191)
 HDAC2 IC₅₀: 4.48 ± 0.79 μM (SI^{2/6}: 107)
 HDAC3 IC₅₀: 8.35 ± 0.06 μM (SI^{3/6}: 199)
 HDAC4 IC₅₀: > 10 μM (SI^{4/6}: > 238)
 HDAC6 IC₅₀: 0.042 ± 0.006 μM

Figure 1.
 Inhibition of HDAC1-3 and HDAC6 by the selected hit compounds **10h** and **10p**. Selectivity index (SI = IC₅₀ (HDAC1, 2, 3, or 4)/IC₅₀ (HDAC6)).

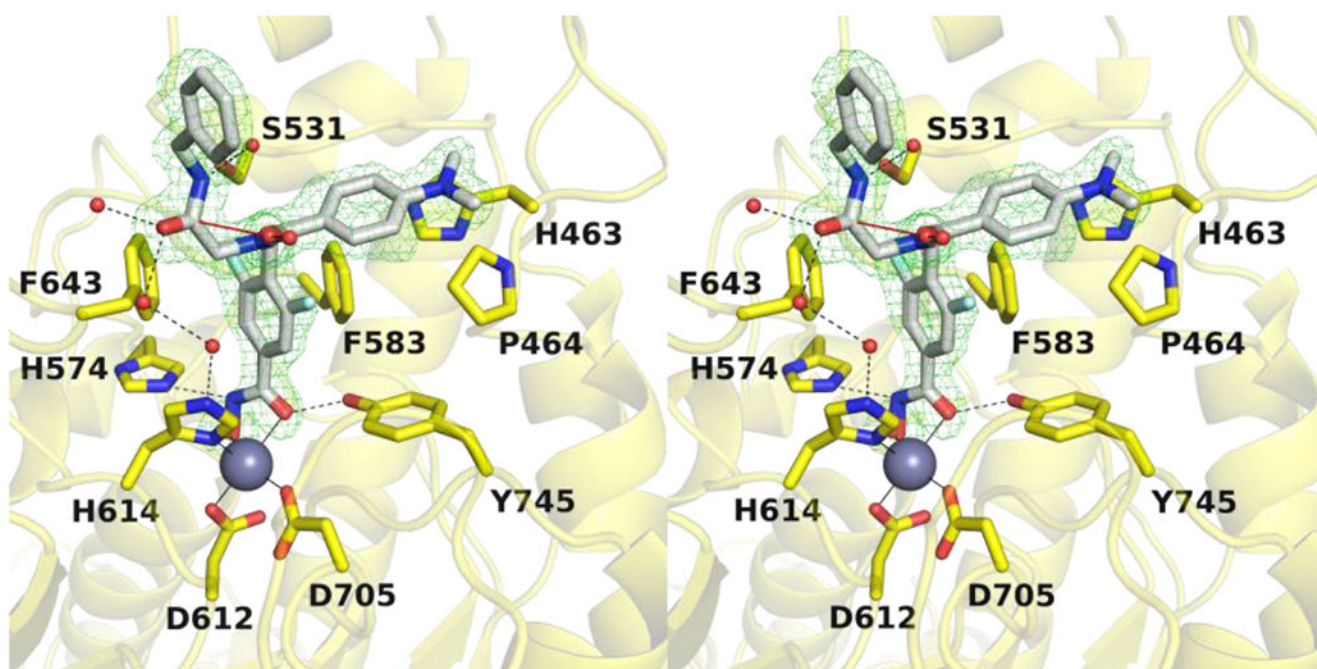


Figure 2. Stereoview of a Polder omit map (contoured at 4.0σ) depicting the bidentate binding mode of **10h** (light gray) in the active site of HDAC6 chain B (yellow) (PDB 7U8Z). Two conformations of the aromatic ring are shown, one with the C–F group oriented into the F583–F643 aromatic crevice, and the other with the C–F group oriented toward solvent. The catalytic Zn²⁺ ion is shown as a grey sphere, and water molecules are shown as small red spheres. Metal coordination, hydrogen bond, and $n \rightarrow \pi^*$ interactions are shown as solid, dashed black, and solid red lines, respectively.

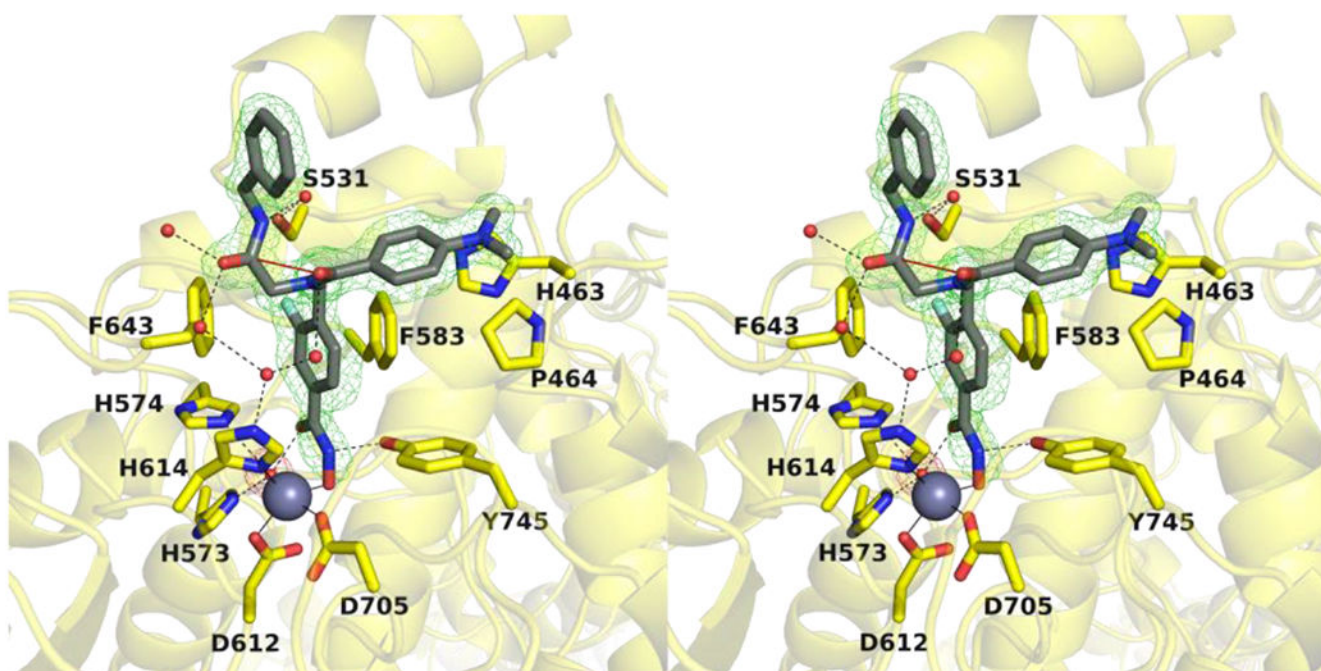


Figure 3. Stereoview of a Polder omit map (contoured at 4.0σ) depicting the monodentate binding of **10h** (dark gray) in the active site of HDAC6 chain D (yellow) (PDB 7U8Z). The catalytic Zn²⁺ ion is shown as a grey sphere, and water molecules are shown as small red spheres. Metal coordination, hydrogen bond, and $n\rightarrow\pi^*$ interactions are shown as solid, dashed black, and solid red lines, respectively.

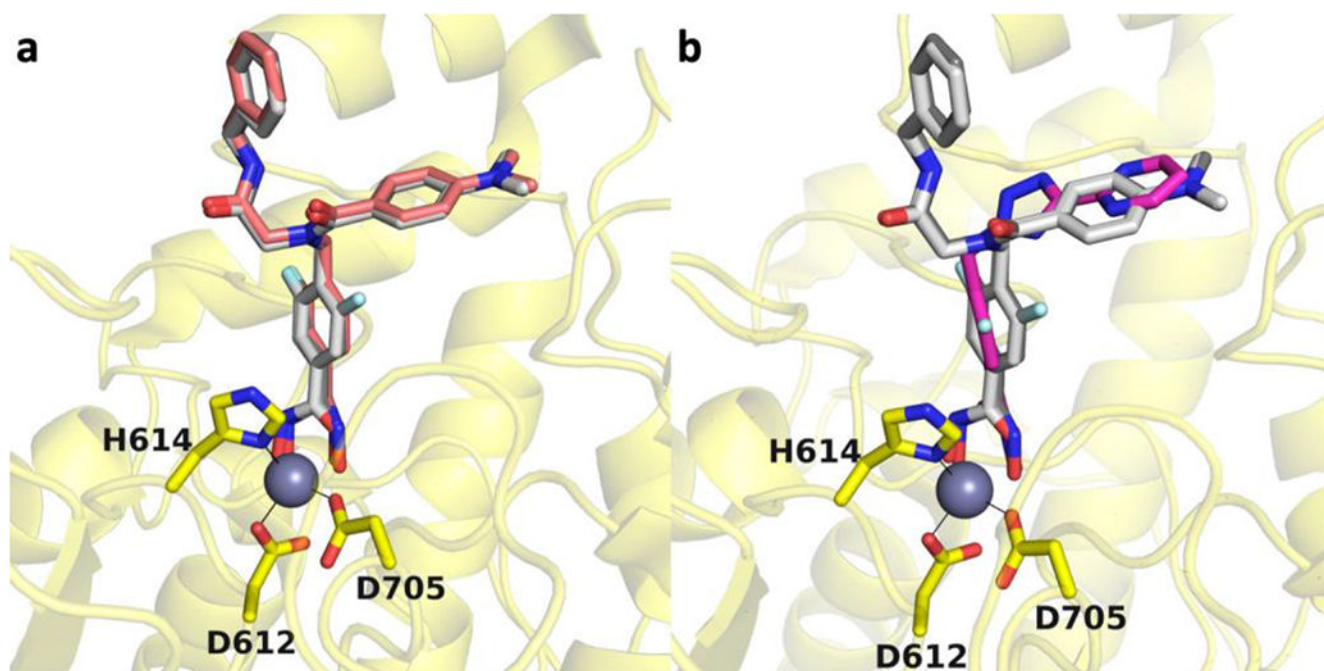
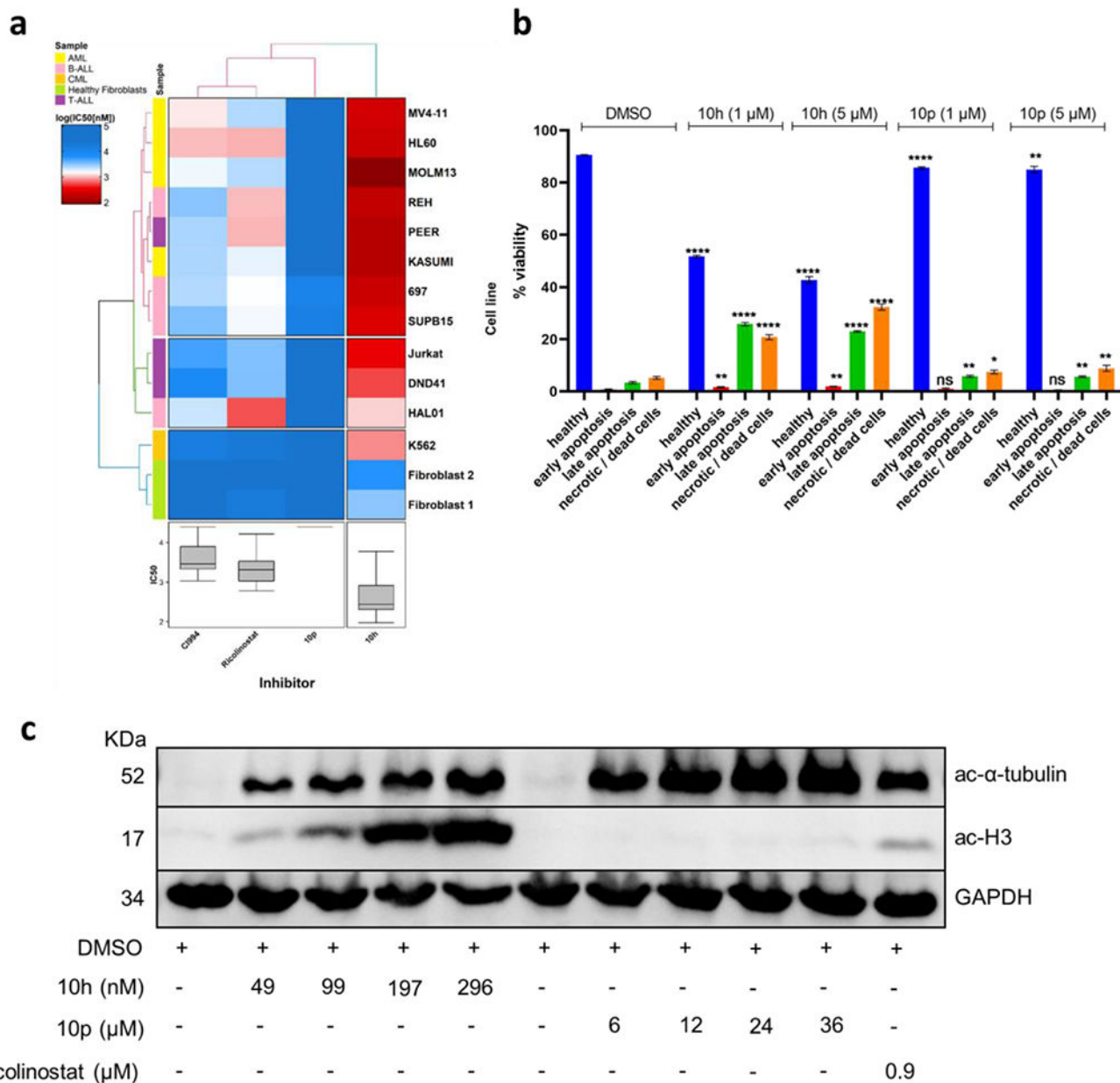


Figure 4.

(a) Overlay of the HDAC6-**10h** complex (chain B, light gray; chain D, dark gray; PDB 7U8Z) with the HDAC6 complex with the non-fluorinated inhibitor (light pink; PDB 6DVN). The catalytic Zn²⁺ ion is shown as a grey sphere and metal coordination is indicated by solid black lines. (b) Overlay of the HDAC6-**10h** complex (chain B, light gray; chain D, dark gray; PDB 7U8Z) with an inhibitor containing a *meta*-difluorophenyl linker (PDB 7O2R).

**Figure 5.**

Cytotoxic and target specificity analysis of compounds **10h** and **10p**. (a) Comparative cellular viability ($\log IC_{50}$ nM) of different subgroups of leukemic cell lines and two healthy human fibroblast controls after treatment with **10h** and **10p** in comparison to the commercially available selective HDAC6 inhibitors ricolinostat and the HDAC class I inhibitor CI994. The IC_{50} data are plotted as a clustered heat map, followed by unsupervised hierarchical clustering. The horizontal axis of the dendrogram exemplifies the dissimilarity between clusters, whereas the color of the cell is related to its position along with a $\log IC_{50}$ (nM) gradient. (b) Annexin-PI staining of HL60 cells exposed to **10h** and **10p** at 1 μ M and 5

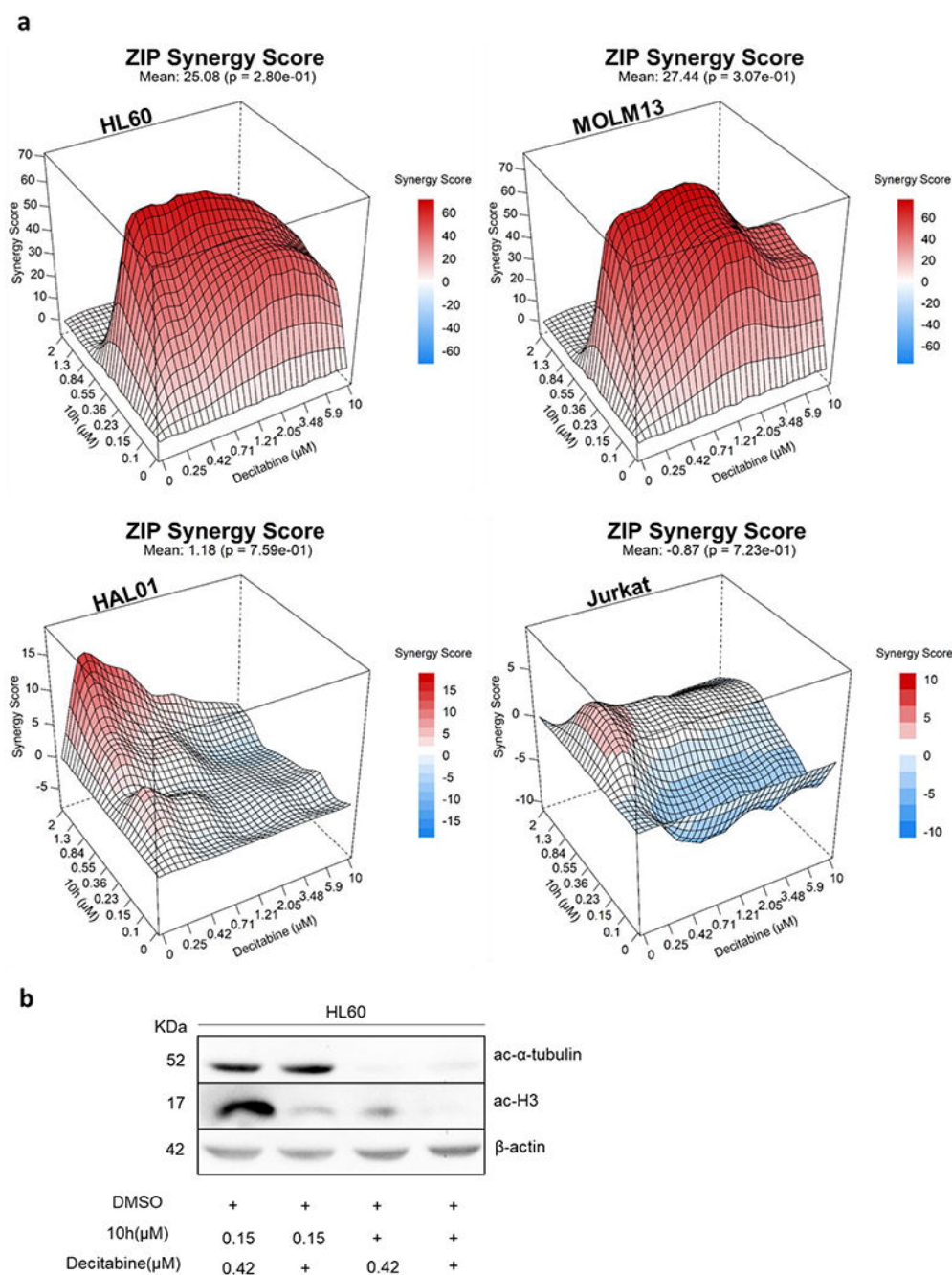
μM after 48 h (n=3). (c) Immunoblot of HL60 cells after 24 h treatment with **10h**, **10p**, and ricolinostat at the indicated concentrations.

Author Manuscript

Author Manuscript

Author Manuscript

Author Manuscript

**Figure 6.**

(a) Illustrative synergy plot of **10h** after 72 h co-treatment of HL60, MOLM13 (AML), HAL01 (B-ALL), and Jurkat (T-ALL) leukemic cell lines with decitabine at depicted concentrations. The mean synergy score calculations were performed using ZIP model; visualizations were carried out using Synergy Finder webtool.⁶² (b) Immunoblotting of HL60 cells after 24 h of treatment with **10h** alone and in combination with decitabine at the indicated concentrations.

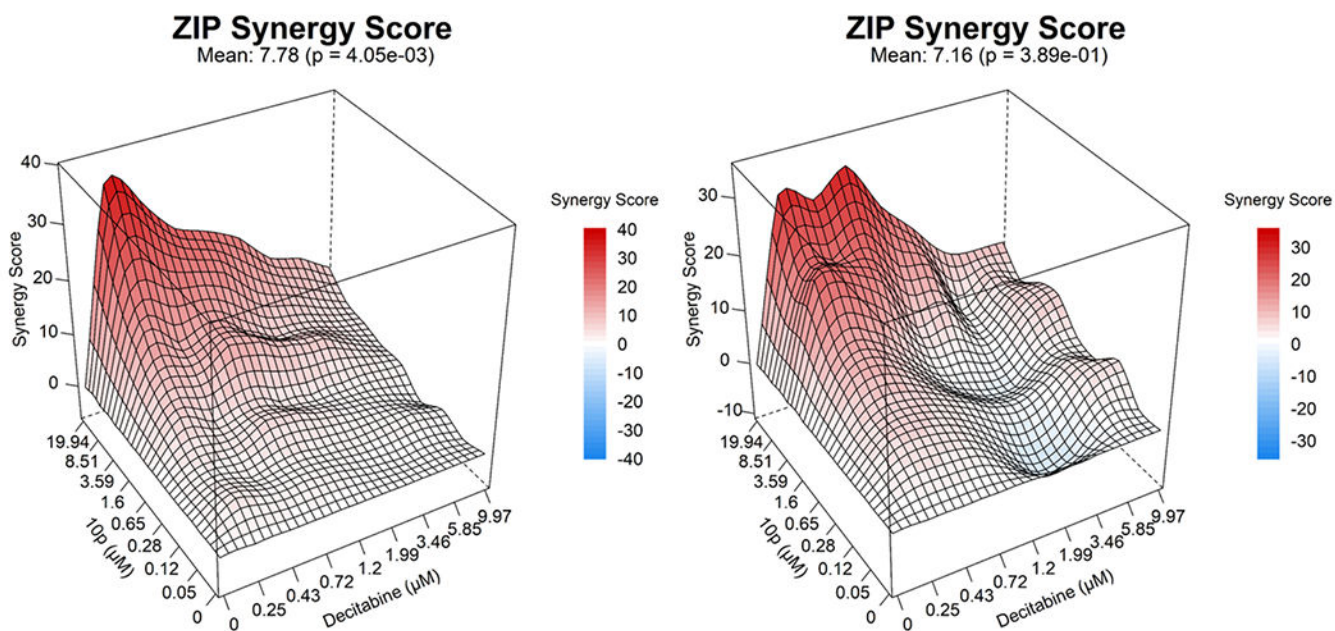
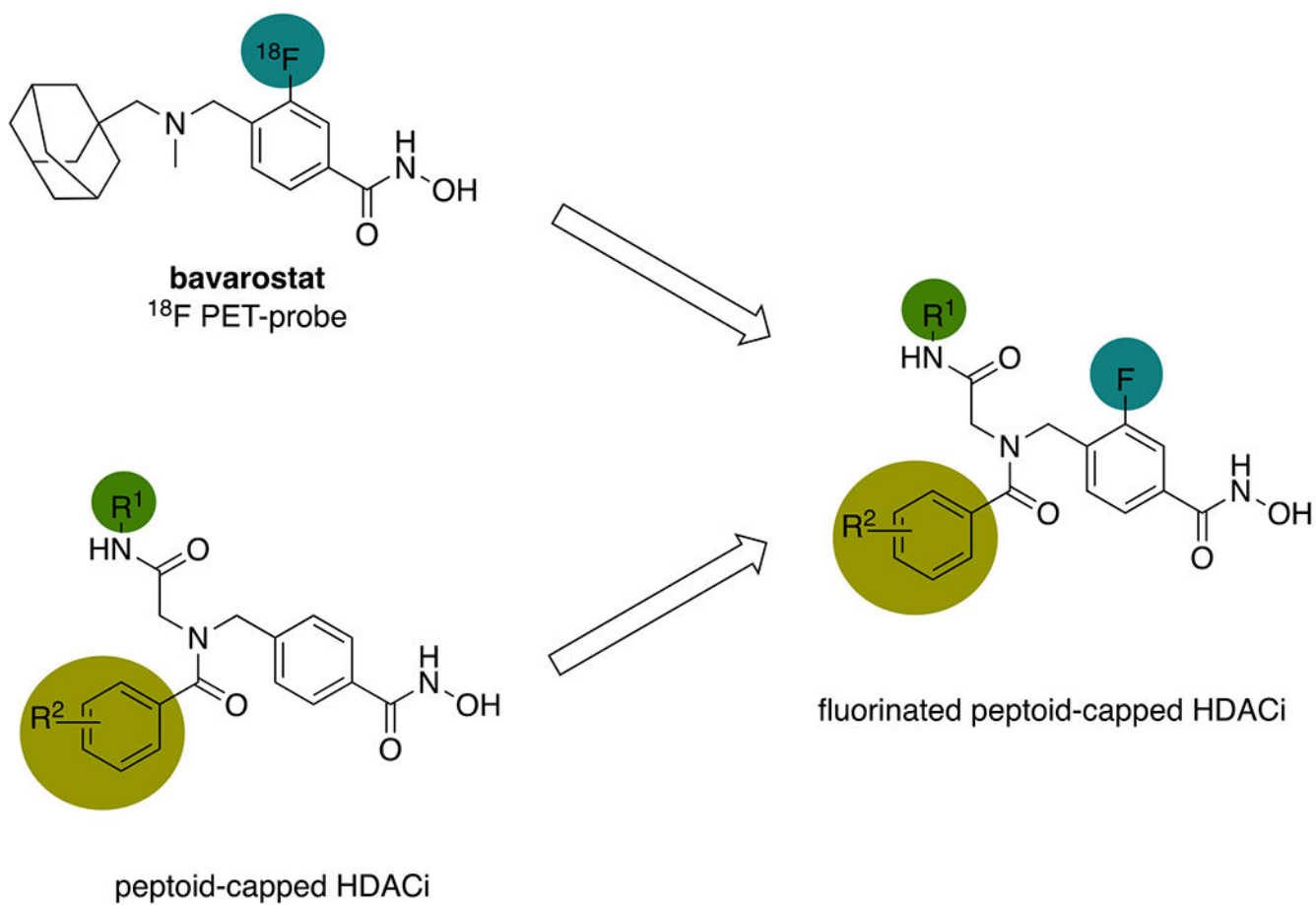
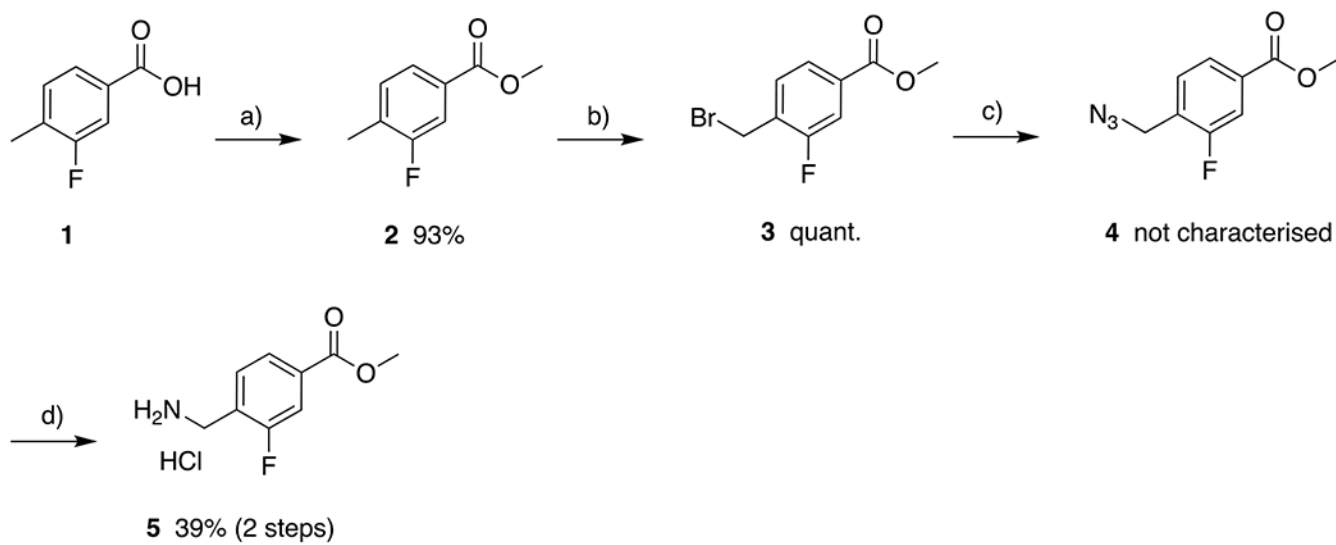


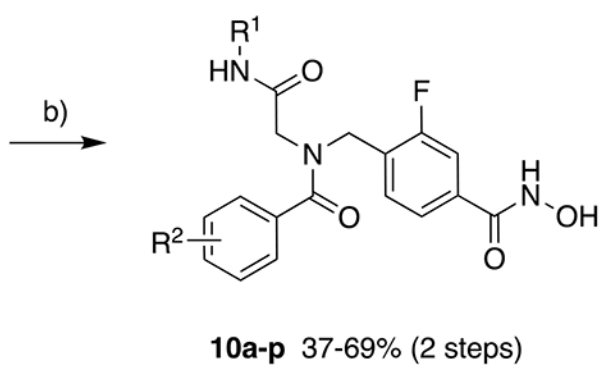
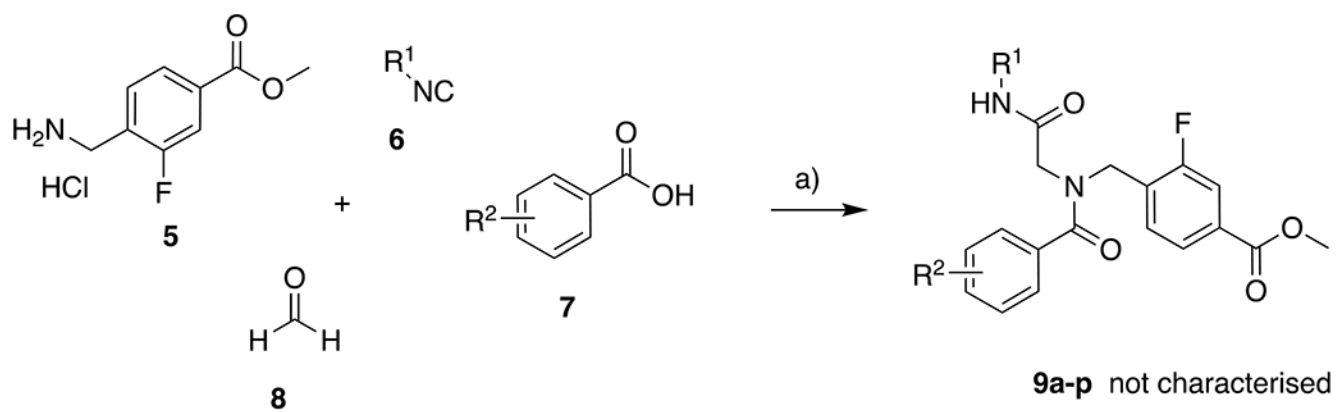
Figure 7:
Illustrative synergy plot of **10p** after 72 h co-treatment of HL60, MOLM13 (AML) leukemic cell lines with decitabine at depicted concentrations. The mean synergy score calculations were performed using ZIP model; visualizations were carried out using Synergy Finder webtool.⁶²

**Scheme 1.**

Design of fluorinated peptoid-capped HDACi inspired by the preclinical PET-probe bavarostat.

**Scheme 2.**

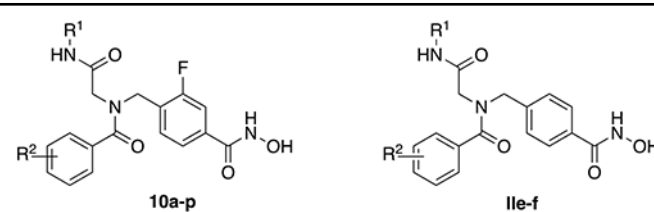
Synthesis of the fluorinated linker **5**. a) SOCl_2 , MeOH, 0 °C to rt, 16 h; b) NBS, AIBN, DCM, reflux, 16 h; c) NaN_3 , DMF, 80 °C, 16 h; d) PPh_3 , HCl, THF, rt, 24 h.

**Scheme 3.**

Synthesis of the fluorinated peptoid-capped HDACi **10a-p**. a) Et₃N, MS 4Å, MeOH, microwave, 45 °C, 150 W, 60–210 min; b) H₂NOH, NaOH, MeOH, DCM, 0 °C, 15 min.

Table 1.

IC₅₀ of the fluorinated HDACi **10a-p** and the non-fluorinated analogs DDK115, DDK137, and **IIe-f** in comparison to vorinostat, ricolinostat, HPOB and Tubastatin A (Tub A) against HDACs 1 and 6.



Compound	R ¹	R ²	HDAC1 IC ₅₀ [μM]	HDAC6 IC ₅₀ [μM]	SI ^a
10a	c-Hexyl	3,5-Me	0.310 ± 0.004	0.020 ± 0.002	16
10b	c-Hexyl	4-NMe ₂	0.066 ± 0.008	0.016 ± 0.004	4
10c	c-Hexyl	2-F	0.771 ± 0.006	0.018 ± 0.002	43
10d	c-Hexyl	2-Me	0.938 ± 0.013	0.018 ± 0.002	52
10e	c-Hexyl	2-OMe	1.50 ± 0.10	0.020 ± 0.004	75
10f	c-Hexyl	2-CF ₃	1.45 ± 0.05	0.027 ± 0.002	54
10g	Bn	3,5-Me	0.077 ± 0.003	0.013 ± 0.004	6
10h	Bn	4-NMe ₂	0.013 ± 0.001	0.010 ± 0.00004	1.3
10i	<i>t</i> -Bu	3,5-Me	0.573 ± 0.011	0.024 ± 0.002	24
10j	<i>t</i> -Bu	4-NMe ₂	0.158 ± 0.056	0.020 ± 0.006	8
10k	<i>t</i> -Bu	2-F	1.18 ± 0.15	0.026 ± 0.002	45
10l	<i>t</i> -Bu	2-Me	1.75 ± 0.13	0.027 ± 0.005	65
10m	<i>t</i> -Bu	2-OMe	1.75 ± 0.05	0.017 ± 0.0001	103
10n	<i>t</i> -Bu	2-CF ₃	2.33 ± 0.43	0.027 ± 0.005	86
10o	<i>t</i> -Bu	2-Cl	3.47 ± 0.14	0.021 ± 0.001	165
10p	<i>t</i> -Bu	2- <i>i</i> Pr	8.01 ± 0.22	0.042 ± 0.006	191
DDK115	c-Hexyl	3,5-Me	0.249 ± 0.028	0.040 ± 0.008	6
DDK137	Bn	4-NMe ₂	0.005 ± 0.0006	0.011 ± 0.003	0.5
IIe ^b	<i>t</i> -Bu	2-Me	2.41 ± 0.086	0.051 ± 0.004	47
III ^b	<i>t</i> -Bu	2-OMe	3.11 ± 0.308	0.038 ± 0.004	82
Vorinostat	-	-	0.099 ± 0.005	0.042 ± 0.005	2
Givinostat	-	-	0.035 ± 0.002	0.014 ± 0.0002	2.5
Givinostat ^c	-	-	0.070 ± 0.012	0.023 ± 0.004	3
Ricolinostat ^d	-	-	0.19 ± 0.022	0.018 ± 0.003	11
Tub A ^e	-	-	2.49 ± 0.14	0.014 ± 0.0006	178
HPOB ^e	-	-	2.10 ± 0.23	0.085 ± 0.009	25

^a: Selectivity index (SI = IC₅₀ (HDAC1)/IC₅₀ (HDAC6)).

^b: Data taken from Reference 46

c. Data taken from Reference 47

d. Data taken from Reference 50

e. Data taken from Reference 51

Author Manuscript

Author Manuscript

Author Manuscript

Author Manuscript

Table 2.

Cytotoxicities of **10a-p** against selected leukemia cell lines. Vorinostat, HPOB, and ricolinostat were used as controls.

Compound	R ¹	R ²	HAL01 IC ₅₀ [μM]	HL60 IC ₅₀ [μM]	Jurkat IC ₅₀ [μM]
10a	c-Hexyl	3,5-Me	3.10 ± 0.91	2.47 ± 2.05	3.91 ± 0.67
10b	c-Hexyl	4-NMe ₂	1.05±0.28	0.494±0.126	0.946±0.087
10c	c-Hexyl	2-F	11.8±5.14	6.79±3.31	8.97±1.73
10d	c-Hexyl	2-Me	9.93±1.55	7.72±3.45	9.47±3.55
10e	c-Hexyl	2-OMe	>25	12.3±9.70	18.6±9.01
10f	c-Hexyl	2-CF ₃	9.12±4.44	2.00±0.80	>25
10g	Bn	3,5-Me	2.75±1.92	9.15±0.28	6.23±1.62
10h	Bn	4-NMe ₂	0.375±0.162	0.218±0.122	0.285±0.064
10i	<i>t</i> -Bu	3,5-Me	4.93±2.60	4.84±2.78	5.47±0.86
10j	<i>t</i> -Bu	4-NMe ₂	2.47±0.74	1.46±0.77	1.74±0.26
10k	<i>t</i> -Bu	2-F	22.2±3.8	15.7±6.87	19.0±4.58
10l	<i>t</i> -Bu	2-Me	23.9±1.54	13.6±8.19	23.9±1.49
10m	<i>t</i> -Bu	2-OMe	>25	18.4±9.34	24.5±0.75
10n	<i>t</i> -Bu	2-CF ₃	>25	18.6±9.05	>25
10o	<i>t</i> -Bu	2-Cl	22.9±2.64	12.8±8.66	21.6±3.37
10p	<i>t</i> -Bu	2- <i>i</i> Pr	>25	12.2±9.36	>25
Vorinostat	-	-	0.299±0.045	0.22±0.05	0.470±0.023
Ricolinostat	-	-	2.04±0.39	1.54±0.16	2.42±0.18
HPOB	-	-	13.9±3.89	11.3±7.2	16.1±2.52